In presenting the dissertation as a partial fulfillment of the requirements for an advanced degree from the Georgia Institute of Technology, I agree that the Library of the Institute shall make it available for inspection and circulation in accordance with its regulations governing materials of this type. I agree that permission to copy from, or to publish from, this dissertation may be granted by the professor under whose direction it was written, or, in his absence, by the Dean of the Graduate Division when such copying or publication is solely for scholarly purposes and does not involve potential financial gain. It is understood that any copying from, or publication of, this dissertation which involves potential financial gain will not be allowed without written permission.

_____

_____

3/17/65
b

THE EXCITATION OF BARIUM IONS BY ELECTRON IMPACT

A THESIS

Presented to

The Faculty of the Graduate Division

by

Frank Mallary Bacon

In Partial Fulfillment

of the Requirements for the Degree

Doctor of Philosophy

in the School of Electrical Engineering

Georgia Institute of Technology

February, 1968

THE EXCITATION OF BARIUM IONS BY ELECTRON IMPACT

Approved:

Chairman

Date approved by Chairman: 2/8/68

ACKNOWLEDGMENTS

It is a pleasure to express my sincere appreciation to my thesis advisor, Dr. J. W. Hooper, for his guidance, assistance and encouragement throughout the performance of this research. I would also like to express my gratitude to Dr. E. W. Thomas who provided many valuable suggestions during the prosecution of the research and the preparation of this manuscript. This manuscript also benefited from the careful reading and invaluable comments of Dr. F. K. Hurd. I would also like to thank Dr. M. T. Elford for his many helpful suggestions and comments during the later phase of data collection and during the preparation of this manuscript.

It is a pleasure to acknowledge the assistance of M. O. Pace during the later developmental phases of the research and during the extensive data collection process. To my fellow graduate students, recently replaced by a chain hoist, I extend my sincere appreciation for the many times they helped me lift the top cover to the vacuum chamber.

I would like to express my appreciation to the Controlled Thermonuclear Research Program, Division of Research, U. S. Atomic Energy Commission for the generous support of this research and for the research assistantship support during the prosecution of the research.

TABLE OF CONTENTS

LIST OF TABLES

LIST OF ILLUSTRATIONS

SUMMARY

A crossed beam technique has been developed for measuring the emission cross section for the excitation of electric dipole transitions in ions by electron impact. The experimental method involves crossing modulated ion and electron beams in a well defined collision volume. A portion of the photon flux radiated from the excited ions is detected at an angle of 90° to the plane of the two beams by direct observation of the collision volume with a photomultiplier tube. The selection of a single emission line is accomplished with an interference filter. The total flux of radiation from the collision volume for a particular transition can be determined with a knowledge of the photon detection probability of the apparatus. The possibility of an anisotropic angular distribution of radiation from the collision volume is evaluated by measuring the polarization fraction. The emission cross section can be determined from the ion and electron beam currents, current density distributions and energies, and the total radiation flux.

This technique has been used to measure the relative emission cross sections for excitation of the resonance transitions in Ba^+ ions by electron impact. The resonance transitions, between the excited $6^2P^o_{1/2}$ and $6^2P^o_{3/2}$ levels and the $6^2S_{1/2}$ ground state, produce photons with wavelengths of 4934 Å and 4554 Å. The thresholds for exciting the $6^2P^o_{1/2}$ and $6^2P^o_{3/2}$ levels are 2.5 eV and 2.7 eV, respectively. Over the energy range of the experiment, from 8 eV to 98 eV, the relative cross sections differ by approximately a factor of two, the ratio of the

statistical weights of the 6P levels. The relative data also exhibit the high energy dependence predicted by the Bethe-Born approximation. From a best estimate of the photon detection probability of the apparatus, estimated absolute cross sections are obtained which agree remarkably well in magnitude and shape with the theoretical predictions. Checks on the data were performed to evaluate the possible effects of such parameters as the beam intensities, beam modulation frequency, ion beam composition, ion beam energy, electron beam energy distribution, beam profiles, and signal-to-noise ratio.

CHAPTER I

INTRODUCTION

A crossed beam technique has been developed to determine the emission cross sections for the excitation of the resonance transitions of Ba^+ ions by electron impact over the energy range from 8 eV to 98 eV. The process can be described by the following equations.

$$e + Ba^+ \rightarrow e + (Ba^+)^* \qquad (1)$$

$$(Ba^+)^* \rightarrow Ba^+ + \text{photon}$$

As shown in the energy level diagram[1] in Figure 1, the resonance transitions occur between the $6^2P^o_{1/2}$ and $6^2P^o_{3/2}$ levels and the $6^2S_{1/2}$ level with wavelengths of 4934 Å and 4554 Å. The thresholds for exciting the $6^2P^o_{1/2}$ and $6^2P^o_{3/2}$ levels are 2.5 eV and 2.7 eV, respectively.

The experimental method involves crossing modulated ion and electron beams in a well defined collision volume. After the ion is excited by collision with an electron, the electric dipole transitions occur before the ion has traveled a millimeter because the lifetimes of the excited states of interest are approximately 10^{-8} seconds[2] and the velocity of the ions is approximately 10^6 centimeters per second. A portion of the radiation from the excited ions is detected by direct observation of the interaction region with a photomultiplier tube

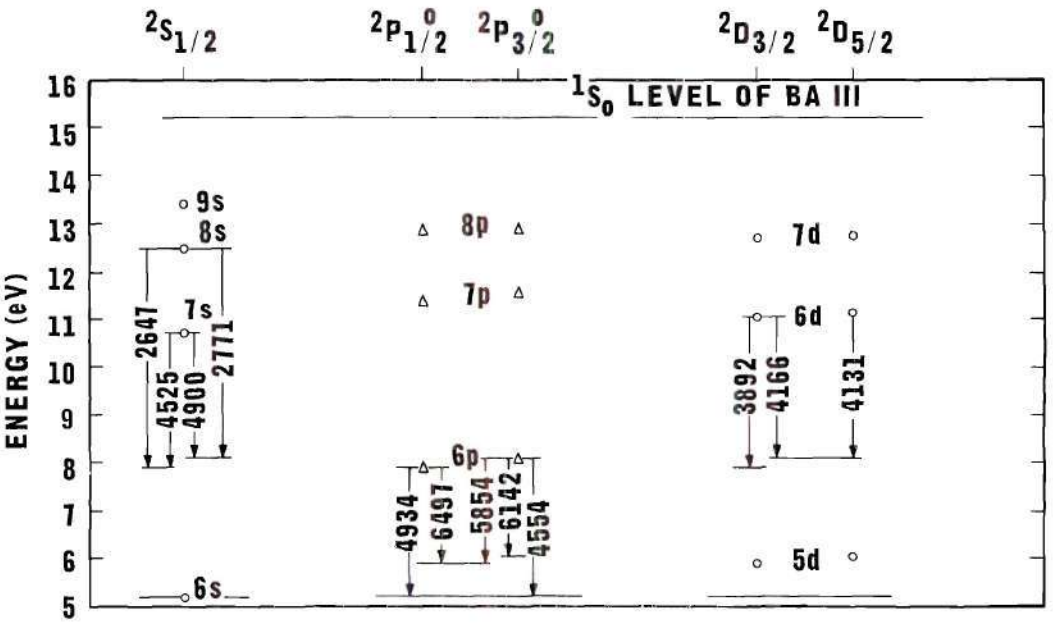

Figure 1. Energy Level Diagram of Ba^+.

operated in a counting mode. The selection of a single resonance line is made with an interference filter. With a knowledge of the photon detection probability and the photon flux angular distribution around the collision volume, the magnitude of the cross sections is determined.

The present results represent the first measurement of an emission cross section for the excitation of electric dipole transitions in an ion by electron impact using crossed beam techniques. Since the first report of this work,[3] others[4] have reported a similar measurement in N_2^+. The development of this measurement technique was the principal motivation for performing the experiment. A practical incentive for obtaining information on the excitation of barium ions by electron impact is related to the use of barium plasmas in certain studies in the controlled thermonuclear research program.[5] Barium is used in these plasma experiments because the resonance lines of the ion are in the blue visible range and are thus convenient for spectroscopic detection while spectrally separated from a large portion of the visible light generated at hot surfaces, and because barium has a sufficiently low ionization potential to be ionized by contact with hot metal surfaces. Fully ionized barium plasmas have been found to yield emission spectra which consist of the two ionic resonance lines at 4554 Å and 4934 Å plus the three ionic lines of the $6^2P \rightarrow 5^2D$ transitions at wavelengths of 6142 Å, 6497 Å, and 5854 Å. Ion density fluctuations in barium plasmas can be studied by observing the fluctuations in the intensities of these self-excited resonance lines.[6] The excitation process occurs primarily by electron impact; therefore, detailed information about the cross sections for excitation of these transitions by

electron impact would be of considerable interest. The cross section information directly applicable to these plasma experiments lies in the low energy range from threshold to approximately five eV. The present cross section data have a lower energy bound of eight eV and are thus not directly applicable to the plasma experiments; however, this experiment does establish a basis for future experimental investigation at lower energies.

Several electron-ion crossed beam experiments have been successfully completed since the pioneering effort of Dolder, Harrison and Thonemann[7] in 1961. A summary of these experiments is given in Table 1.

Table 1. Summary of Electron-Ion Crossed Beam Experiments

Process	Target	Authors	Reference
Ionization	He^+	Dolder, Harrison and Thonemann	Proc. Roy. Soc. (London) A-264, 367 (1961).
Ionization	Ne^+	Dolder, Harrison and Thonemann	Proc. Roy. Soc. (London) A-274, 546 (1963).
Ionization	N^+	Dolder, Harrison and Thonemann	Proc. Phys. Soc. (London) 82, 368 (1963).
Ionization	Hg^+ and Noble Gas Ions	Latypov, Kupriyanov and Tunitskii	J. Expt. Theoret. Phys. (U.S.S.R.) 46, 833 (1964); English transl.: Soviet Phys.--JETP 19, 570 (1964).
Ionization	Li^+	Lineberger, Hooper and McDaniel	Phys. Rev. 141, 151 (1966).
Ionization	Na^+ K^+	Hooper, Lineberger and Bacon	Phys. Rev. 141, 165 (1966).

Table 1. Summary of Electron-Ion Crossed Beam Experiments (Continued)

Process	Target	Authors	Reference
Excitation	He^+	Dance, Harrison and Smith	Proc.Roy.Soc.(London) A-290, 74 (1966).
Dissociation	H_2^+	Dunn and Van Zyl	Phys.Rev. 154, 40 (1967).
Dissociation	H_2^+	Smith, Dance, Harrison and Rundel	V International Conference on the Physics of Electronic and Atomic Collisions, Leningrad, U.S.S.R., July 17-23, 1967, Abstracts of Papers.
Detachment	H^-	Tisone and Branscomb	Phys.Rev.Letters 17, 236 (1966).
Detachment	O^-	Tisone and Branscomb	V International Conference on the Physics of Electronic and Atomic Collisions, Leningrad, U.S.S.R., July 17-23, 1967, Abstracts of Papers.
Detachment	H^-	Dance, Harrison and Rundel	Ibid.
Excitation	Ba^+	Bacon and Hooper	Ibid.
Ionization	Li^+	Wareing and Dolder	Proc.Phys.Soc. (London) 91, 887 (1967).
Excitation	N_2^+	Lee and Carleton	Bull. Amer. Phys. Soc. (To be published).
Dissociation	N_2^+	Van Zyl and Dunn	Phys. Rev. 163, 43 (1967).
	O_2^+		

Excellent discussions of the experimental technique and associated problems are presented by several authors.[8,9,10]

The experiment of Dance, Harrison and Smith[11] on the excitation of the 2S level of He^+ by electron impact represents the only crossed beam study of ion excitation completed prior to the present work. It should be noted, however, that there is a basic difference between the work of Dance, *et al.*, and the present results on the excitation of Ba^+. The 2S level examined in their experiment is metastable, and consequently, observation of the desired transitions may be made in a quench field located a sufficient distance downstream from the interaction region to permit the decay of the ordinary excited states before the ions reach the quench region. Such a technique appears possible only for hydrogenic structures which have ordinary excited levels lying very close to the metastable levels. The application of an electric field to such excited ions can lead to sufficient overlap of the wave functions of the metastable and optically permitted levels to permit quenching of the metastable state. In contrast, direct observation in or near the interaction region is required in the study of ordinary excited ions.

The theoretical interpretation of excitation of atoms and ions by electron impact is limited because of the complexity of the calculations and the lack of adequate atomic wave functions to describe the collision process. The status of the theory is in general poor due to the many approximations which must necessarily be invoked in the detailed calculations. Only the more simple ionic structures, the isoelectronic sequences of hydrogen,[12,13,14] helium[15] and lithium,[16,17]

have been studied in much detail. Electron impact excitation of the 4S → 4P and 3D → 4P transitions in Ca^+ near threshold have been studied by Van Regemorter;[18] this appears to be the most complex ion given any detailed theoretical analysis.

The only theory presently applicable on the excitation of Ba^+ by electron impact is the general quantum mechanical treatment of excitation developed by Bethe[19] and modified by Seaton.[20] The semi-classical collision theory of Gryzinski[21] should also be applicable to Ba^+ at high electron energies.

CHAPTER II

EXPERIMENTAL TECHNIQUE

In the previous chapter, the process for the production of electric dipole radiation by ion-electron impact is described. In this chapter, the technique for measuring the cross section for this process is discussed. Attention is paid to the theory of the experiment and to the basic processes contributing to the measured cross section such as cascading effects and polarization.

Consider a monoenergetic singly ionized ion beam and a monoenergetic electron beam traveling parallel to the X and Y axes, respectively, of a rectangular coordinate system. Let V_i and V_e be the ion and electron velocities. If both beams are sufficiently tenuous that multiple collisions can be neglected, then the cross section for the production of electric dipole radiation by ion-electron impact is shown* to be

$$\sigma_{em} = \Phi_T \frac{e^2 V_i V_e}{(V_i^2 + V_e^2)^{1/2}} \frac{F}{I_i I_e} \qquad (2)$$

where

---

*This expression is derived in Appendix I.

$$F = \frac{\int_{-\infty}^{\infty} i_i(z)dz \int_{-\infty}^{\infty} i_e(z)dz}{\int_{-\infty}^{\infty} i_i(z)\, i_e(z)\, dz}, \qquad (3)$$

Φ_T is the total flux of photons emitted from the collision volume, I_i is the total ion beam current, I_e is the total electron beam current, e is the magnitude of the electronic charge, and $i_i(z)dz$ and $i_e(z)dz$ are the ion and electron currents passing through the region z to z + dz.

The cross section in Equation (2), σ_{em}, is defined here as an emission cross section because the process described by Equation (1) results in the emission of a photon. Actually, as indicated by Equation (1), the emission cross section represents a two-step process: the excitation of a given level and then the decay of that excited state by the emission of a photon. The excited state, i, may become populated by direct excitation from the ground state by electron impact or by cascading transitions from higher energy states, p, which were excited from the ground state by electron impact. Generally, the excited state can decay to more than one state; as shown in Figure 1, the $6^2P^o_{3/2}$ state of Ba^+ can decay to one of three different states: the $6^2S_{1/2}$ state, the $5^2D_{3/2}$ state or the $5^2D_{5/2}$ state. In such cases, a branching ratio, $\gamma(i \rightarrow j)$, is defined as the ratio of the number of transitions from state i to state j to the total number of transitions from state i to all possible states. The emission cross section can be represented in terms of these processes as

$$\sigma_{em}(6^2P_J^o \rightarrow 6^2S_{1/2}) = \gamma(6^2P_J^o \rightarrow 6^2S_{1/2}) \left[\sigma_{ex}(6^2S_{1/2} \rightarrow 6^2P_J^o)\right. \tag{4}$$

$$\left. + \sum_p \gamma(p \rightarrow 6^2P_J^o)\ \sigma_{ex}(6^2S_{1/2} \rightarrow p)\right]$$

where J = 1/2 or J = 3/2, $\gamma(i \rightarrow j)$ is the branching ratio for electric dipole transitions from state i to state j, and $\sigma_{ex}(m \rightarrow n)$ is the cross section for excitation from initial state m to final state n. The sum over p is taken over all states, p, with energies higher than the $6^2P_J^o$ state. This sum represents the cascading contribution to the excitation of the $6^2P_J^o$ level.

Radiation emitted as a result of particle impact often exhibits polarization effects[22] determined by the direction of the particle beam which produces the excitation. Let $\phi_{\parallel}$ and $\phi_{\perp}$ be the photon fluxes observed at an angle of 90° to the exciting beam with electric vectors parallel and perpendicular to the direction of the exciting beam, respectively. Then the polarization fraction P is defined as

$$P = \frac{\phi_{\parallel} - \phi_{\perp}}{\phi_{\parallel} + \phi_{\perp}} . \tag{5}$$

In electric dipole radiation the angular distribution of the radiation flux is given by the equation

$$\phi(\theta) = \frac{\Phi_T}{4\pi} \frac{3(1 - P\cos^2\theta)}{3 - P} \tag{6}$$

where $\phi(\theta)$ is the photon flux per unit solid angle emitted in the direction between θ and $\theta + d\theta$, and Φ_T is the total flux. The angle θ is measured with respect to the exciting beam, in this case, the electron beam.

Only a fraction of the total photon flux from the collision volume is detected by the photomultiplier tube. The photocathode is centered on the Z-axis, $\theta = 90^\circ$, at a distance z_o from the interaction region, thus the fraction of the total radiation, A, collected by the photocathode is given by

$$A = \frac{a}{4\pi z_o^2} \tag{7}$$

where a is the area of the photocathode. If the photomultiplier tube counting efficiency is E, then the photon detection probability, η, is given by

$$\eta = A E. \tag{8}$$

The signal, S, from the detection system is thus given by

$$S = 4\pi \phi(90^\circ)\eta = \frac{3\eta}{3 - P} \Phi_T. \tag{9}$$

Solving this equation for Φ_T and substituting into Equation (2) gives the emission cross section in terms of the experimentally observable quantities.

$$\sigma_{em} = \frac{S}{\eta} \frac{3 - P}{3} \frac{e^2 V_i V_e}{(V_i^2 + V_e^2)^{1/2}} \frac{F}{I_i I_e} \tag{10}$$

The program for the experimental determination of σ_{em} was

(1) Measurement of the relative cross section expressed as

$$\sigma_{em}^R = \frac{3\eta}{3 - P} \sigma_{em} = \frac{S F}{I_i I_e} \frac{e^2 V_i V_e}{(V_i^2 + V_e^2)^{1/2}} , \tag{11}$$

(2) Measurement of the polarization fraction, P, and

(3) Evaluation of the photon detection probability, η.

The parameters in Equation (11) most difficult to determine accurately are the form factor F and the signal S. The form factor is evaluated approximately* as shown in Figure 2 by scanning both beams simultaneously using an L-shaped probe with coplaner slits similar to those used by others.[7,9,10,11] An alternative procedure for obtaining F utilizes the top of the probe to measure the integral of the current distributions. Differentiation of the resulting data then gives the distribution functions $i_i(z)$ and $i_e(z)$. As Dunn and Van Zyl[10] have discussed, equivalence of the two methods is taken as evidence that possible errors resulting from differences in space charge due to probe positions, possible image charges on the probe, or insulating layers on the probe surface are not important. The possibility of errors in measuring F decrease with increasing uniformity of the ion beam if the

*See Appendix 1.

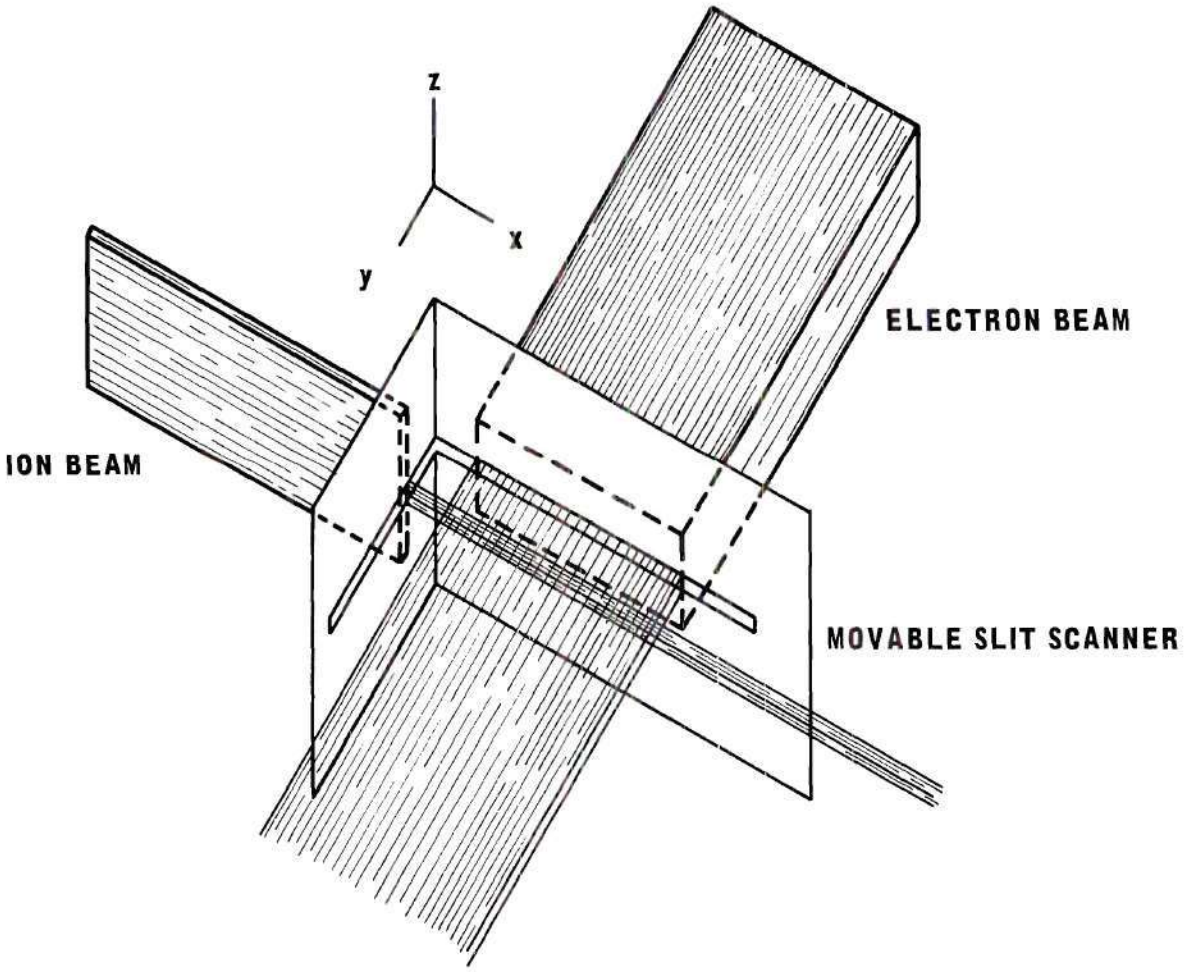

Figure 2. Use of a Movable Slit Scanner to Determine Beam Profiles.

electron beam is well contained inside the ion beam. These constraints allow for space charge expansion of the electron beam as it travels through the interaction region and also for a possibility that the axis of the electron beam may be slightly nonparallel to the Y-axis. The slit scanner technique has been carefully evaluated by Dunn and Van Zyl even without the above constraints on the beams, and, under their operating conditions, was shown to be accurate to ±1 per cent. Since F could not be varied over a significant range in the present experiment, the precaution was taken to maintain the electron beam inside a uniform ion beam.

The evaluation of S would be simple were it not for sources of photons of identical or approximate wavelengths as that of the signal. This flux of photons, identified here as noise, is often a factor of 100 times the signal. An effective method for extracting the signal from this noise is the double beam modulation system described in the following chapter.

In this crossed beam experiment, the electron velocity V_e is much greater than the ion velocity V_i. Under this condition the relative velocity of an ion and an electron is essentially the electron velocity; therefore, the total energy in the center-of-mass reference frame is very nearly equal to the laboratory energy of the electron. Since the cross section should be a function only of the total center-of-mass energy, the measured cross sections should remain constant as the ion energy is varied, provided that the electron energy is fixed. For a given electron energy the measured cross sections should be independent of changes in the electron beam intensity, the ion beam intensity, and the form

factor F. The variation of each of the parameters in Equation (11) provides a valuable check on some aspects of the performance of the experimental apparatus. The results must also be independent of other experimental parameters not contained in this equation, such as the beam modulation frequency and the magnitude of the noise.

The polarization fraction P is determined from the measurement of $\phi_{\parallel}$ and $\phi_{\perp}$ by introducing a polarizing film between the collision volume and the photomultiplier tube so that the polarizing axis is first parallel and then perpendicular to the direction of the electron beam. The finite solid angle at $\theta = 90^{\circ}$ subtended by the detection system gives a value of P that is less than the theoretical P which is evaluated at $\theta = 90^{\circ}$ and zero solid angle. Since the signal is measured with this same finite solid angle, the measured value of P is the proper value to use when correcting for the anisotropy in the photon flux distribution introduced by the polarization.

To obtain an absolute cross section, the photon detection probability η can, in principle, be measured by determining the response of the experimental system to a source of known luminosity, such as a black body radiator. No such direct calibration is made in the present work; instead, the photon detection probability is estimated by evaluating the solid angle subtended by the detection system and estimating the transmission of the windows and filters and the quantum efficiency of the photomultiplier tube from manufacturer's data. The results are termed an "estimated absolute cross section," thereby reserving the term "absolute cross section" for those cases where the calibration is determined by proper standards.

CHAPTER III

EXPERIMENTAL APPARATUS

The measurement of the emission cross sections using the technique described in the previous chapter was the objective of the present experiment. In this chapter, the experimental apparatus necessary to perform these measurements is described.

A schematic diagram of the experimental apparatus is presented in Figure 3. In the diagram the slit scanner is shown in position for scanning the beams; during measurement of parameters other than the form factor, the scanner was raised out of the interaction region. The apparatus used for producing and collecting the ion and electron beams is attached to an experiment plate which is bolted to the top cover of a vacuum chamber. This apparatus is then suspended inside the vacuum chamber which is evacuated to pressures of the order of 10^{-9} torr. The current measuring apparatus and the photon detection system are located outside the vacuum chamber. A viewing port in the chamber cover permits the direct observation of the beam interaction region. An overall view of the experimental apparatus is shown in Figure 4. The vacuum system control instrumentation is on the left of the vacuum chamber, while the instrumentation for the actual experiment is on the right. The remainder of this chapter is concerned with a detailed description of the construction and operation of each of the major components of the experimental apparatus.

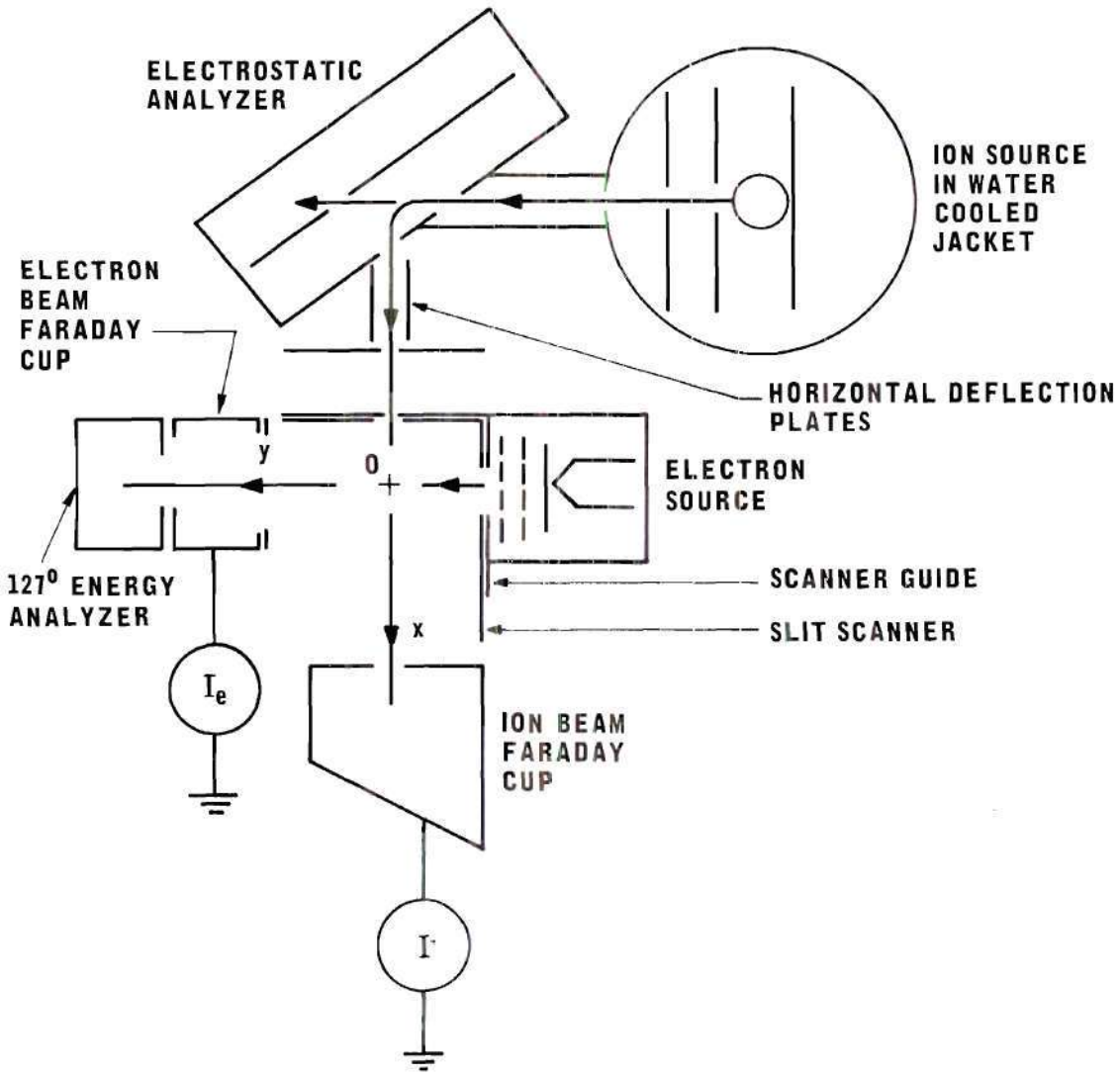

Figure 3. Schematic Diagram of Experimental Apparatus.

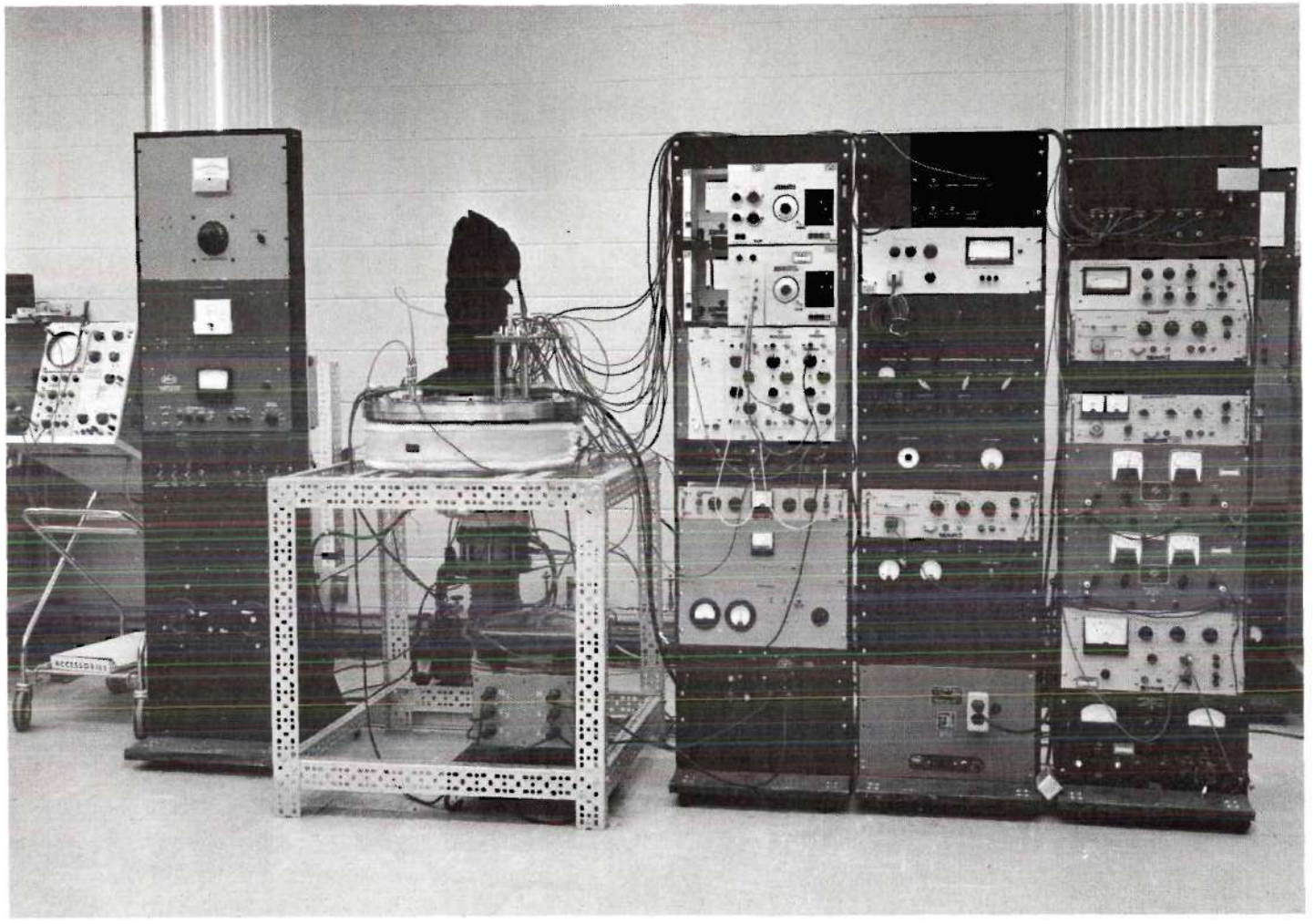

Figure 4. Overall View of Experimental Apparatus.

Vacuum System

The vacuum enclosure is an all stainless steel bakable chamber 21 inches in diameter by 6 inches deep. Most of the vacuum seals are metal o-ring compression seals using soft aluminum wire; the flange around the viewing port is a Varian "Conflat" flange. The pumping system consists of a four-inch oil diffusion pump, a water cooled chevron baffle and a zeolite molecular sieve trap. No cryogenic trapping is employed in the vacuum system. Details of the vacuum system are contained in the Ph.D. Thesis of W. C. Lineberger[23] and will not be repeated here.

Bakeout Procedure and Vacuum System Performance

The zeolite trap and vacuum chamber walls were heated to approximately 370°C and 170°C, respectively, for a period of 36 to 48 hours. During this period of time the ion source was heated to its operating temperature and the electron source was activated. When room temperature was reached following bakeout, with one milliampere of electron current and 10^{-7}A ion beam current, the indicated pressure was 2 - 3 x 10^{-8} torr. After several days of operation under these conditions the pressure continued to decrease to 5 - 7 x 10^{-9} torr. No significant deterioration in this performance was evident over a period of at least one month. With both the electron source and the ion source cold, the base pressure in the chamber was approximately 2 x 10^{-9} torr.

Ion Beam Source and Optics

Three types of ion sources were considered for this experiment: the electron bombardment source, thermionic source, and surface ioniza-

tion source. The electron bombardment source was eliminated because of the uncertainty in the state of excitation of the emerging ion beam, for example, the metastable 5^2D levels of Ba^+ might be excited.

Initially, attempts were made to develop a thermionic source of barium ions similar to others which have been reported in the literature. Because of insufficient current intensities and source lifetime, this type of source was abandoned.

Surface ionization proved to be a satisfactory method of obtaining an ion beam of the order of 10^{-7}A with a lifetime of the order of weeks and operable in an ultra high vacuum chamber. The final version of this source, shown in Figure 5, utilizes surface ionization of neutral barium on a hot rhenium filament. Barium metal is evaporated from a molybdenum crucible which is heated to approximately 600°C by a tungsten filament electrically insulated from the crucible by a thin coating of alumina. The crucible is 3/8 in. OD, 1/4 in. ID by 1 in. long. The rhenium filament, with dimensions of 0.002 in. x 1/8 in. x 1 in., is secured at both ends in iron clamps which serve as electrical connections and mechanical supports. The filament is heated to approximately 1800°C by a direct current of 15 to 18 amperes. Initially, an alternating current was used to heat the filament but the voltage across the filament was sufficient to modulate the ion beam current at the line frequency. The barium gas diffuses into the region around the filament through a 1/8 in. diameter hole in one of the end plates; this plate offers thermal isolation between the crucible and the filament. This thermal isolation is necessary to maintain the crucible of barium at the desired temperature and hence maintain the desired rate of evapora-

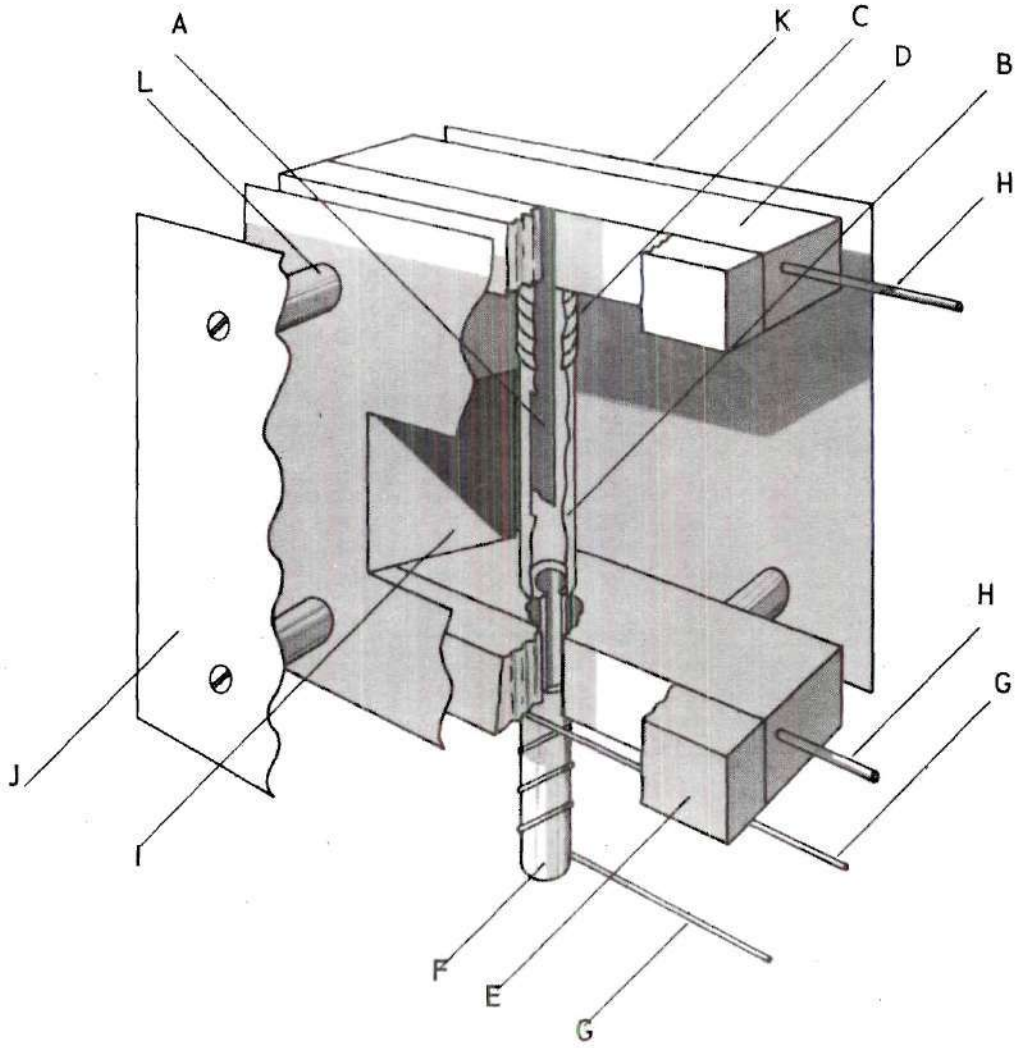

(A) SURFACE IONIZATION FILAMENT
(B) MOLYBDENUM SLEEVE (WITH SLIT)
(C) ALUMINA SLEEVE
(D) UPPER CLAMP FOR FILAMENT
(E) LOWER CLAMP FOR FILAMENT
(F) MOLYBDENUM CRUCIBLE
(G) CRUCIBLE HEATER
(H) CURRENT LEADS FOR FILAMENT
(I) EXTRACTION ELECTRODE
(J) EXIT ELECTRODE
(K) REPELLER ELECTRODE
(L) INSULATING SPACER

Figure 5. Surface Ionization Source for Barium Ions.

tion. Around the filament is a molybdenum tube of 0.003 in. wall thickness with a 1/16 in. x 3/4 in. slit through which the ionized barium is extracted. The ionizing filament is held at the desired positive acceleration potential of the beam while the extraction electrode is biased negatively approximately 50 volts with respect to the filament. This bias is used to control the intensity of the ion beam. The exit electrode is held at ground potential while the repeller electrode is maintained at the acceleration potential. An ion current of the order of 10^{-7} A is obtained at an acceleration potential of 500 to 1000 volts.

The ion beam purity was checked on a magnetic sector mass spectrometer. The results of this test showed that the only source of contamination was the rhenium filament which emitted potassium and sodium ions. After operating the source for approximately two hours the beam current contamination decreased to less than 1 per cent. After eight to ten hours of operation, the contamination decreased to 0.2 per cent and was still decreasing. Since the ion source was run continuously in the vacuum chamber for a period of at least three days before any cross section data were taken, the contamination is estimated to be less than 0.1 per cent of the total ion beam current. Since the beam contamination contributes nothing to the signal, the only error introduced is in the measurement of the ion beam current.

The possibility of the ion beam being metastably excited must be considered because the energy levels of the $5^2D_{3/2}$ and the $5^2D_{5/2}$ states lie only 0.6 eV and 0.7 eV, respectively, above the $6^2S_{1/2}$ ground state level. If the ions achieve thermal equilibrium with the surface of the

ionizing filament at a temperature of 2100°K, then, from Boltzmann statistics, 7 per cent of the beam would be excited to the $5^2D_{3/2}$ state and 6 per cent of the beam would be excited to the $5^2D_{5/2}$ state. The spontaneous emission transition probabilities for the $5^2D_{3/2} \rightarrow 6^2S_{1/2}$ and the $5^2D_{5/2} \rightarrow 6^2S_{1/2}$ transitions have been calculated[24] to be 0.014 sec^{-1} and 0.030 sec^{-1}. Assuming the ions are in the radiation field of a 2100°K blackbody and using the above emission transition probabilities, the transition probabilities for the $6^2S_{1/2} \rightarrow 5^2D_{3/2}$ and the $6^2S_{1/2} \rightarrow 5^2D_{5/2}$ transitions are 0.001 sec^{-1} and 0.002 sec^{-1}, respectively. The extraction field of the ion source, of the order of one volt per centimeter, extracts the ion from the source in approximately 10^{-5} seconds. The length of time that the ion remains in the source is, therefore, insufficient for the ion to reach thermal equilibrium with the rhenium filament or to become metastably excited by radiation absorption. The voltage drop across the rhenium filament, approximately five volts, is too small to cause any metastable excitation problems by electron impact. The ion beam is considered, therefore, to be in the ground state.

The source is enclosed in a copper covered 4-3/4 in. length of 3 in. diameter stainless steel pipe which is wrapped with 1/4 in. stainless steel tubing. By water cooling this container, operating pressures with beams on of 5×10^{-9} torr were achieved. Lower pressures were difficult to achieve because of the low ionizing efficiency of the source. An attempt to improve this efficiency was made by using iridium in place of rhenium, but the higher vapor pressure of iridium precluded a sufficiently long life for the filament.

The feedthrough for the cooling water to the ion source and the current to the oven and ionizing filament of the ion source was made on a blank 4 in. flat flange. Welded to the flange were four ADVAC type 375-ES cable end seals for current feedthroughs and two 6 in. lengths of 1/4 in. stainless steel tubing for water feedthroughs. The ion source cooling coil was connected to the tubing on the feedthrough by a Matheson type 350 gas connection made of 304 stainless steel. To obtain a leakfree joint, an indium gasket was crushed between the nipple and seat of this fitting. The mounted feedthrough is shown on the left of Figure 6.

After the ion beam emerges from the water-cooled source, it passes through a short piece of tubing to an inclined parallel plate electrostatic analyzer.[25] The tubing connecting the source with the analyzer is used to minimize light leakage from the source to the chamber. The first plate of the analyzer contains the entrance and exit apertures and is at ground potential. The second plate of the analyzer, held at approximately 80 per cent of the ion beam acceleration voltage, contains one aperture which is aligned with the entrance aperture of the first place. This aperture is added to allow passage of neutral barium and photons from the ion source through the analyzer. The second plate of the analyzer is covered, thus the analyzer acts as a neutral particle and photon trap. Exiting the analyzer, the beam passes through parallel plate horizontal and vertical deflection structures used for pulsing and steering the beam. Aperture plates are placed between the analyzer and the interaction region to collimate the beam to dimensions of approximately 3 mm wide by 1 cm high.

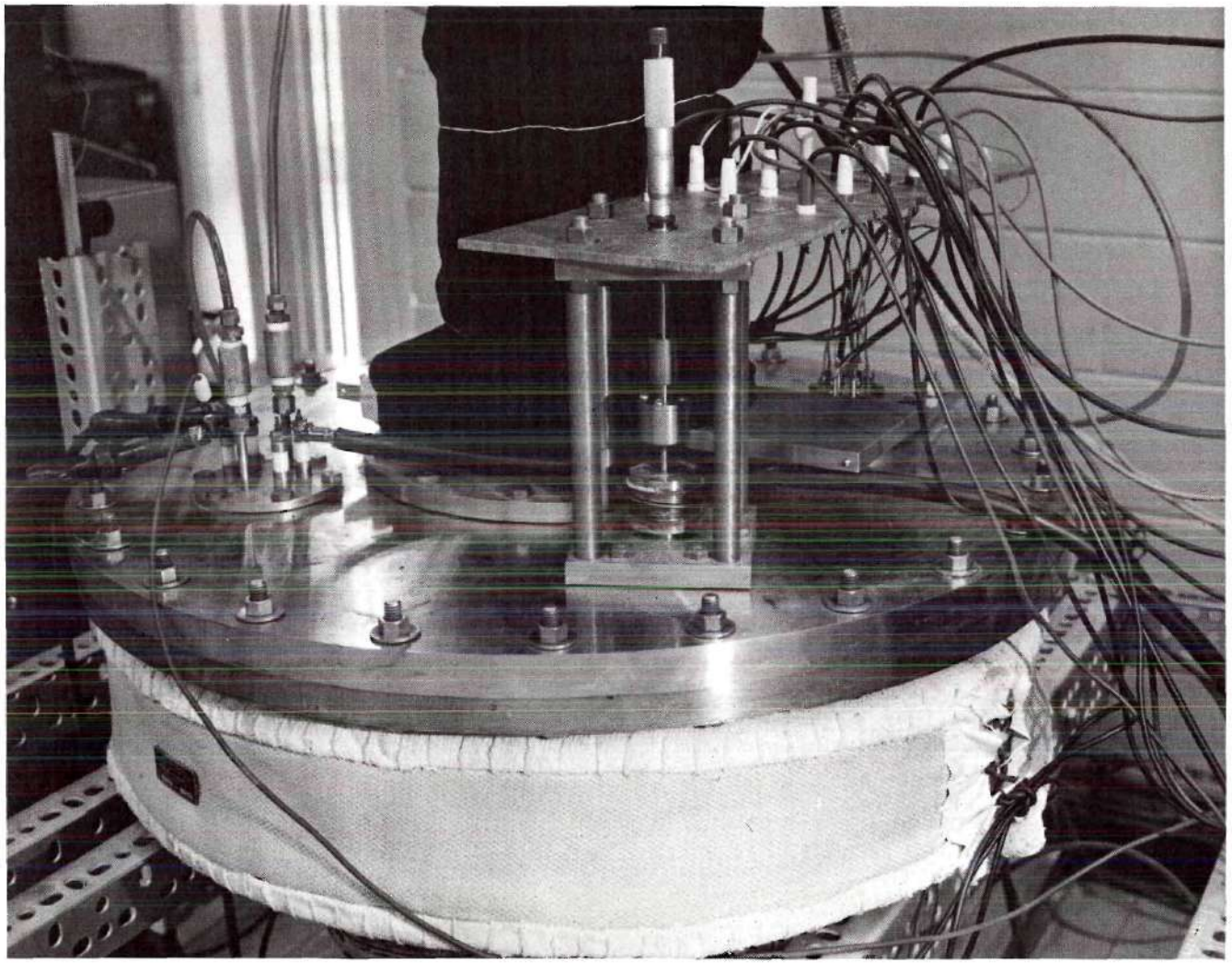

Figure 6. Close-up View of Vacuum Chamber. Scanner Drive is on Right, Ion Source Feedthrough is on Left, and Photomultiplier Tube Cooler and Light-tight Slide are in Background.

As seen in the schematic diagram in Figure 3, the ion faraday cup is a deep cup with the surface being struck by the ion beam inclined with respect to the beam. The solid angle subtended by the entrance to the cup at the region where the ion beam strikes the cup is less than 1 per cent of the total solid angle. In addition, secondary electron and reflected ion suppression structures are incorporated into the cup, but it has been demonstrated that the cup is essentially 100 per cent efficient in retaining reflected and secondary charged particles even when no voltages are applied to the suppression electrodes. Under operating conditions with both the ion and electron beams on, an electron current, of the order of several per cent of the ion beam current, was striking the ion faraday cup. This current, a negligible fraction of the total electron beam current, was partially composed of "cold" electrons and partially energetic electrons with the energy of the electron beam. To eliminate this stray electron current, the ion cup was held at a potential of -120 volts. At this potential, secondary electrons were ejected from the cup. This problem was eliminated by placing the suppressor electrode in the cup at -300 volts. At these potentials, it was demonstrated that the cup was collecting all the ion beam current while not picking up any stray electron current. To keep electric fields at the ion cup out of the interaction region, a plate, at ground potential, was placed between the ion cup and the interaction region. The aperture in this plate is larger than the entrance to the ion cup and large enough to ensure that none of the ions in the beam are intercepted prior to entering the cup. Furthermore, optical alignment of the collimating apertures of the ion source

showed that no ion could be intercepted by this plate.

The average value of the ion beam current was measured with a Keithley 417 Picoammeter. The accuracy of this instrumentation, periodically checked with a Gyra Model CS-57 current source, is better than ±2 per cent. The indicated ion beam energy was set with a John Fluke Model 413D voltage supply with an accuracy of ±0.25 per cent. This accuracy was periodically verified with a John Fluke Model 871A differential voltmeter. The actual ion beam energy is estimated to be within ±1 per cent of the indicated energy; this allows for the voltage across the ionizing filament to be superimposed on the acceleration voltage.

Electron Source

The electron source is a modified 6L6GC beam power tube similar to the one used in earlier work.[9,23] A beam power tube was chosen for the source since it is designed to produce an approximately rectangular electron beam. The 6L6GC is prepared for use in the following manner. The tube base is removed by unsoldering the base pins from the pins in the tube envelope; this gives an excellent means for making electrical connections to the tube. The glass envelope is removed with care not to break the glass base to the envelope. One side of the plate structure is cut and folded back, exposing the cathode and grids. The folded back portion of the plate structure is bent into a position for spot welding to a mounting bracket. The mounted electron source is then properly positioned with respect to the ion beam inside the electron source housing. The major axis of the electron source cathode was fixed

parallel to the axis of the ion beam. The electron beam was then collimated to approximately two centimeters along this axis and centered on the interaction region; no collimation was used along the other axis of the beam. The electrons are accelerated from the negative cathode to ground potential. The beam forming plates are set at cathode potential, the screen grid is at ground potential, and the control grid is used to adjust the electron beam intensity and to pulse the beam. Details of the electron source activation procedure are given elsewhere.[23,26]

Electron Beam Faraday Cup and Electrostatic Energy Analyzer

A schematic diagram of the faraday cup and energy analyzer is shown in Figure 7. The electron beam is collected in a faraday cup which has two suppression electrodes perpendicular to the beam. The first electrode is a nickle grid with 85 per cent transmission; the second electrode is a stainless steel plate with an aperture to allow part of the beam to pass through. In line with this aperture is an aperture in the rear of the electron cup through which approximately 1 per cent of the electron beam passes when no suppression voltage is applied to the second electrode of the faraday cup. This sample of the electron beam, taken along the major axis of the beam, enters a 127° cylindrical electrostatic energy analyzer where the energy distribution of the electron beam can be determined. An aperture plate is placed in front of the electron cup; this is used to give an indication of the space charge divergence of the electron beam as it traverses the interaction region. During data collection, the current to this plate is only a few per cent of the total electron beam current and is included

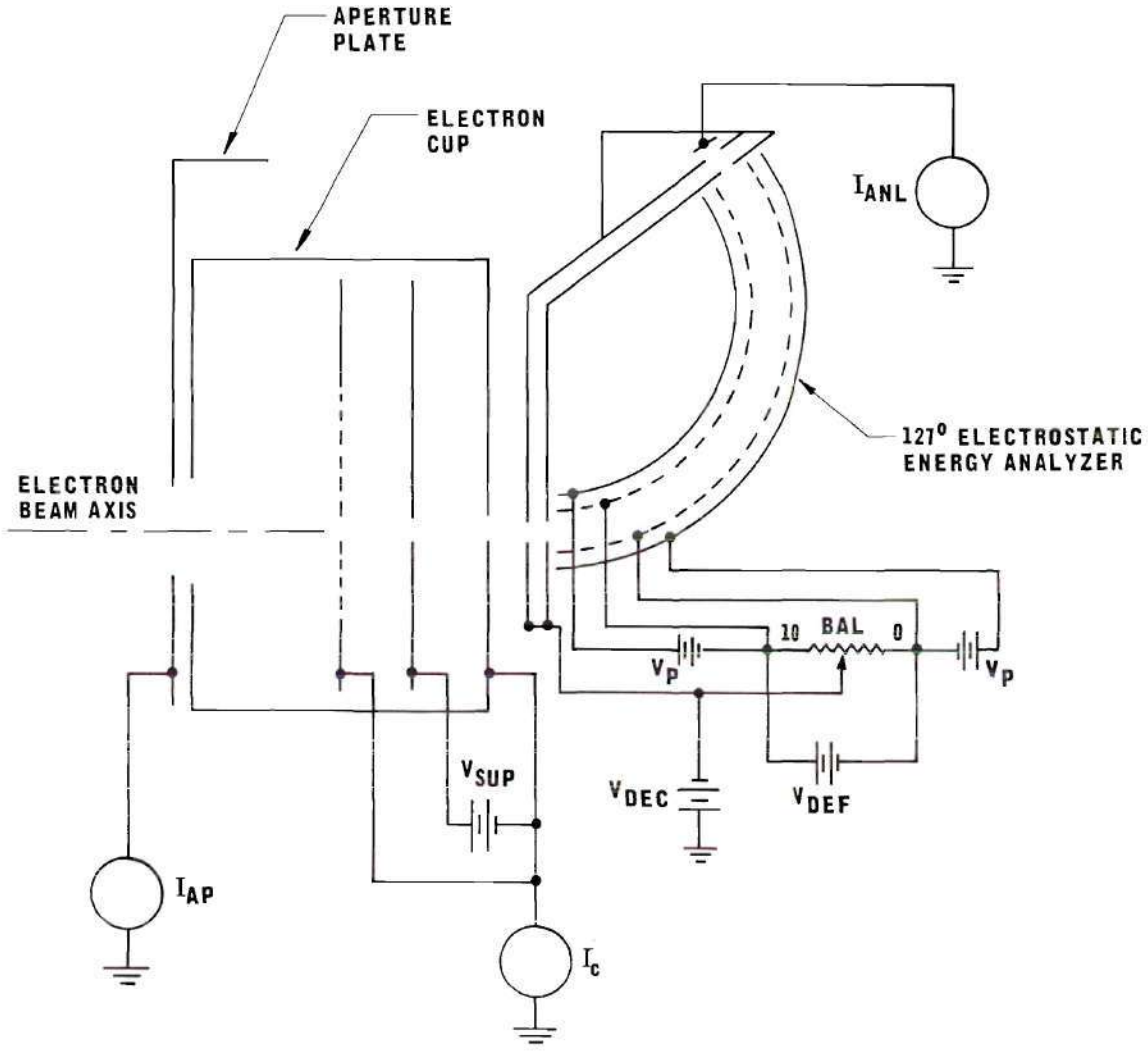

Figure 7. Schematic Diagram of Electron Cup and 127° Electrostatic Energy Analyzer.

in the total beam current measurement.

Initially, the average value of the pulsed electron current was measured with a precision ten ohm resistor and a Keithley Model 149 Milli-Microvoltmeter. When this arrangement was found to be picking up a spurious response to frequency components of the pulsed beam and giving a +13 per cent error in the measurement, a Keithley Model 410 Micro-Microammeter was substituted. The response of this instrument was slow compared to the rise time of the electron beam, thus introducing voltage spikes of up to 40 volts on the electron cup. By passing the current from the cup through a low pass filter, where the output of the filter was the average value of the input current, either of these instruments would perform satisfactorily. The accuracy of the electron current measurement, periodically checked with a Gyra Model CS-57 current source, is better than ±2 per cent. The indicated electron energy was set with a John Fluke Model 413C voltage supply with an accuracy of ±0.25 per cent for voltages which are multiples of ten volts. This accuracy was periodically checked with a John Fluke Model 871A differential voltmeter.

The electrostatic energy analyzer is similar to the improved version of the Hughes and Rojansky analyzer[27] described by Marmet and Kerwin.[28] This analyzer is used to measure the energy distribution of the electron beam and, in particular, to measure where the peak of the energy distribution occurs with respect to the indicated electron beam energy. An energy degradation of a few eV is typical of an oxide coated cathode. The analyzer was constructed by clamping the entrance and exit plates and the cylindrical grids and plates between two

rectangular pieces of supramica. Grooves were machined in the supramica to provide the proper spacing for the electrodes. The radii of the cylindrical grids are 1-13/32 in. and 1-19/32 in. and the entrance and exit apertures are 0.020 inch wide and lie on a 1-1/2 in. radius circle. These dimensions give a theoretical resolution of[27]

$$\frac{\Delta V}{V_{an}} = 0.013 \tag{12}$$

where ΔV is the voltage resolution and V_{an} is the voltage of the electrons in the analyzer.

The analyzer, with the exception of the current collection electrode, can be raised to a negative potential with the deceleration voltage, V_{dec}. Since the voltage of the electrons in the analyzer is given by

$$V_{an} = V_e - V_{dec} \tag{13}$$

where V_e is the electron acceleration voltage applied to the electron source cathode, the resolution of the analyzer may be varied by adjusting the deceleration voltage. The negative deceleration potential also reduces secondary and scattered electrons at the current collection electrode. By adjusting the voltage across the two concentric grids, V_{def}, only the electrons with a prescribed energy exit the analyzer. The electrons retained in the analyzer pass through the grids and are collected by the outside plates held at a positive potential, V_p, with

respect to the grids. The energy of the electrons that pass through the analyzer are related to the voltage across the grids by

$$V = \chi V_{def} \tag{14}$$

where χ can be determined analytically from the geometry of the analyzer or experimentally. The constant χ also depends on the potential of the entrance and exit slit with respect to the field in the analyzer. This relative potential is varied by adjusting the balance potentiometer, BAL. An examination of the fields around the entrance and exit apertures shows that when the balance potentiometer is set at zero a larger deflection voltage is necessary for a given electron to pass through the analyzer than if the potentiometer is set at ten. Therefore, χ_0 is less than χ_{10}, where the subscript denotes the position of the balance potentiometer. Because of uncertainties in the geometrical dimensions of the analyzer and because of the end field effects, an experimental determination of χ was necessary. Measuring an energy distribution for two different deceleration voltages and assuming the peak of the distribution occurs at the same voltage below the acceleration voltage gives two equations in two unknowns from which χ can be determined. If E is the voltage difference between the acceleration voltage and the voltage, V_o, where the peak of the energy distribution occurs, then E and χ are determined from the following set of equations.

$$\left.\begin{aligned} V_{o1} &= \chi\, V_{def-1} = V_e - V_{dec-1} - E \\ V_{o2} &= \chi\, V_{def-2} = V_e - V_{dec-2} - E \end{aligned}\right] \qquad (15)$$

The deceleration voltage, V_{dec}, could be set to ±1 per cent while the deflection voltage across the grids could be set to ±0.3 volts with resettability of ±0.05 volts. To minimize the error in the energy distribution due to errors in the deflection voltage, the lowest value of χ was used in measuring most of the distributions; i.e., the balance potentiometer was set at the zero position.

Interaction Region

The interaction region was designed to provide a field free space for intersection of the ion and electron beams. The interaction region is defined by a T-shaped bracket to which the ion beam collimating structure and the electron source are secured and on which the moveable slit scanner rides. The slit scanner should intercept the ion and electron beams as close to the interaction region as possible; in this experiment the scanner intercepts the two beams approximately 3/8-inch prior to their intersection. The slit height on the scanner is 0.020 inch. The linear motion of the scanner is introduced by means of a metal bellows assembly positioned with a micrometer drive, shown in Figure 6. The scanner was also built so the leading edge could be used to measure an integral current distribution. This distribution when differentiated should give the same results as the differential distribution measured directly with the slit. Errors, in addition to

the possible errors associated with the differential scanning procedure, might be introduced with the numerical differentiation which requires taking differences of large numbers. Throughout the experiment the difference in the measured form factor using these two procedures was less than 2 per cent. Form factors taken routinely with the differential method were reproducible to better than 1 per cent. The error associated with the form factor measurement is estimated to be no larger than ±2 per cent.

Detection System

The photon detection system consists of a set of lens, a vacuum chamber window, interference filter and a photomultiplier tube housed in a thermoelectric cooler. The output of the tube is processed for counting with a preamplifier, amplifier and pulse height analyzer.

The lens system is shown in Figure 8. The dimensions of the collision volume are approximately 3 mm wide by 2 cm long by 3 mm deep. The first lens focuses an image of the collision volume approximately 2.5 cm above the window. This lens is made from two plano-convex lenses having a 55.0 mm focal length and a 42.0 mm diameter. The window is a Granville-Phillips 1-1/2 inch diameter model with a 2 mm thick type 7056 Pyrex glass. The second lens is a single plano-convex lens identical to those described above. Its purpose is to collimate the light from the image of the collision volume so that it passes perpendicularly through the face of the interference filter. The filter, made by Thin Film Products, Inc., has a full-width-half-maximum of approximately 50 Å, a full-width at 1 per cent transmission of approximately 175 Å,

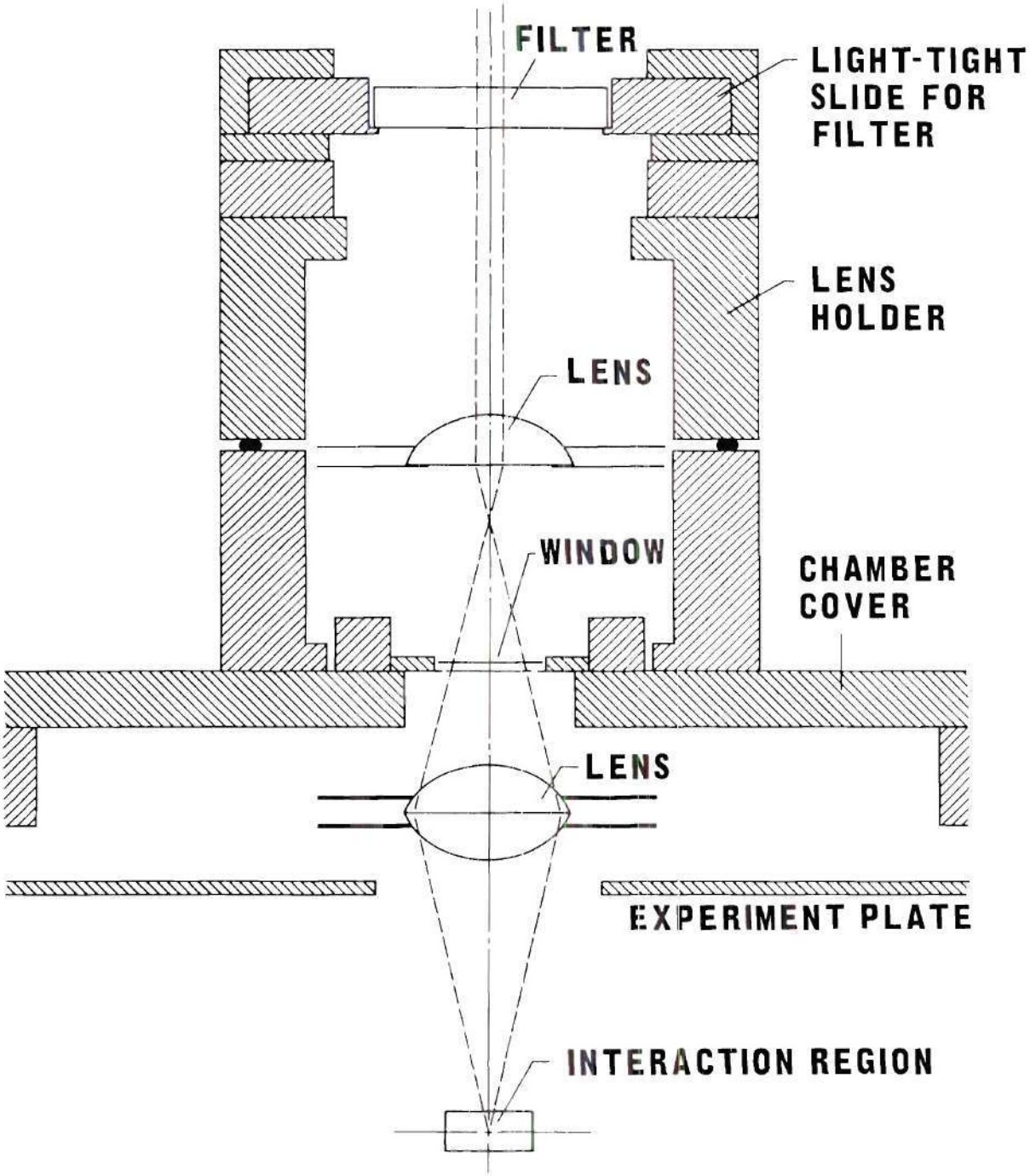

Figure 8. Schematic Diagram of Lens System.

and a peak transmission of over 60 per cent. The transmission characteristics of each filter were measured over the range of 3000 Å to 6000 Å to check for spurious transmission peaks. The transmission outside a 600 Å passband was found to be less than 0.5 per cent, thus the filter for one resonance line rejects the other resonance line by a factor of over 10^3. To facilitate interchanging filters, a light-tight slide[29] is used to hold the filters in place. The housing for the photomultiplier tube is located above the light-tight slide with the photocathode approximately 14 cm above the filter.

To achieve the proper focusing and collimation of the light from the collision volume, the positions of the lenses were empirically determined on an optical bench. The final alignment was made with the lens in position on the experiment. This alignment was accomplished by placing a small lamp in the interaction region and centering a piece of polar graph paper at the location of the photocathode. By positioning the lamp at different points in the interaction region, it was possible to show that, from any point in the collision volume, the light from the lamp was focused and collimated so that it would strike the photocathode. Apertures were arranged at the window so that no light from the electron source was directly focused on the photocathode. The focusing lens inside the vacuum chamber is rigidly attached to the experiment plate and was not moved once alignment was completed. The collimating lens outside the chamber is rigidly attached to its housing which is fitted to the chamber cover so that disassembly of the apparatus will not alter the alignment. The light-tight slide, rigidly attached to the photomultiplier tube housing, is also fitted to the lens housing so that

alignment is maintained.

The output of the photomultiplier tube, an EMI 9584S, is processed for counting with an RIDL Model 10-17 preamplifier and an RIDL Model 33-13A counter-pulse height analyzer combination. The counts are registered in an RIDL Model 49-25 timer-scaler. Because the signal and noise originate from similar sources, the pulse height distributions of the two are identical. For this reason, the analyzer is operated in an integral mode with the threshold set at the sensitivity level.

Interference plagued the counting equipment at the beginning of the experiment. Power line transients, especially from a nearby elevator, were a source of interference that was eliminated by using power line filters. The other major source of interference was the horizontal sync signal from a local television station; this was overcome by shielding the preamplifier with screen wire and by enclosing all the coaxial cable between the preamplifier and amplifier in metal braid. Good grounding techniques were necessary to eliminate both sources of interference.

Beam Modulation System

The signal-to-noise ratio, S/N, the stability of the signal and noise, and the sources of noise are parameters to evaluate in choosing a particular modulation scheme. For example, if S/N is large enough and both the signal and noise are sufficiently stable, no modulation is necessary and the experiment may be run with continuous beams. If modulation is necessary and if the magnitude of the noise from one beam

is negligible compared to the signal, then the low-noise beam is the only beam that need be modulated provided modulation does not introduce errors in the evaluation of the signal or noise. If the noise from both beams is comparable in magnitude with the signal and depends upon certain operating conditions, then double beam modulation is necessary. This latter case is discussed in more detail in the remainder of this section since it applies to the present experiment.

The sources of noise which led to the choice of the modulation scheme used in this experiment were:

1. A significant fraction of the residual gas in the vacuum chamber was neutral barium which escaped from the ion source. Upon impact by electrons, some of the barium was ionized and excited, thus producing photons against which the interference filters did not discriminate. This noise, N_e, was in phase with the electron beam and was a function of the electron beam current and energy as well as the barium partial pressure.

2. Noise in phase with the ion beam, N_i, was produced when the projectile ion collided with the background gas. These collisions could produce noise photons by exciting the projectile ion or by ionizing and exciting the neutral barium as discussed above.

3. Light from the ion and electron sources was also a source of noise photons. The light from the ion source was reduced to a satisfactory level by shielding and by use of baffles. Necessarily, the electron source is near the interaction region. This resulted in a source of noise that could never be eliminated but was significantly reduced by collimation around the detector and by a reduction of the

operating temperature of the source cathode consistent with good performance.

4. Light leakage around the detector was a source of noise that was virtually eliminated by proper optical shielding.

5. Thermal noise at the photocathode of the photomultiplier tube was satisfactorily reduced by cooling the tube to approximately -20°C in a thermoelectric cooler.

The background noise, N_b, is a sum of all the noises given in paragraphs (3), (4) and (5). Of the background noise, approximately 85 per cent can be attributed to light from the electron source; the remaining 15 per cent comes from the ion source and the noise sources of paragraphs (4) and (5) above.

Typical noise count distributions are listed in Table 2. N_b was determined by counting for a period of 15 minutes with both the electron beam and the ion beam off. N_e was determined by counting for 15 minutes with only the electron beam on and subtracting N_b from the final count. Similarly, N_i was determined with only the ion beam on.

At a pressure of 5×10^{-9} torr, turning off the ion beam resulted in a 10 per cent drop in indicated pressure while turning off the electron beam resulted in a 2 per cent drop in pressure. If the experiment were run in a continuous beam mode, these pressure changes would give a 10 per cent error in the measurement of N_e and a 2 per cent error in N_i. If S/N were 10^{-1}, these errors could lead to as much as a 25 per cent error in the measurement of the signal. Because of these errors introduced by pressure modulation, it was necessary to modulate both beams such that the period of modulation of both beams was short compared to

Table 2. Typical Noise Count Distributions

(a) As a Function of Pressure; λ = 4554 Å

Electron Energy	Pressure: 2 X 10^{-8} torr			Pressure: 7 X 10^{-9} torr		
	20 eV.	50 eV.	100 eV.	20 eV.	50 eV.	100 eV.
N_e	15 %	57 %	63 %	3 %	10 %	24 %
N_i	5 %	3 %	3 %	3 %	3 %	2 %
N_b	80 %	40 %	34 %	94 %	87 %	74 %
N_T	38,000	75,000	88,000	36,000	40,000	42,000

(b) As a Function of Wavelength, λ

Electron Energy	λ = 4934 Å			λ = 4554 Å		
	20 eV.	50 eV.	100 eV.	20 eV.	50 eV.	100 eV.
N_e	1 %	4 %	7 %	3 %	10 %	24 %
N_i	1 %	1 %	1 %	3 %	3 %	2 %
N_b	98 %	95 %	92 %	94 %	87 %	74 %
N_T	81,000	85,000	88,000	36,000	40,000	42,000

N_e - Electron Beam Noise

N_i - Ion Beam Noise

N_b - Background Noise

N_T - Total Noise Count to "Noise" Scaler During a 15-Minute Counting Period

$N_T = N_e + N_i + N_b$

the pressure time constant of the chamber, i.e.

$$\tau_m << \frac{V}{S} \tag{16}$$

where S is the pumping speed, V is the volume of the vacuum chamber and τ_m is the modulation period. The pressure time constant for the vacuum system used in this experiment is approximately 0.1 second. The modulation period was varied from 4 to 32 milliseconds. As will be shown later, the modulation criterion of Equation (16) is sometimes not adequate to overcome pressure modulation in a volume of the size of the beam interaction region.

Basically, the modulation scheme is to square wave modulate or chop both beams and switch the output of the photomultiplier tube between two scalers in phase with the modulation signal so that the signal plus noise is registered in one scaler while the noise is registered in the other scaler. This is shown schematically in Figure 9.

An examination of Table 2 shows that the noise of the electron beam, N_e, is the largest source of beam-dependent noise. Any error in evaluating this noise will reflect as a much larger error in the signal. Fortunately, N_i is relatively small and is not as difficult to evaluate as N_e. To ensure that the signal-plus-noise scaler registers the same N_e as does the noise scaler, the electron beam is modulated so that both scalers operate under identical electron beam configurations. This is achieved by chopping the electron beam at twice the frequency of the ion beam. The electron beam can then be on during either the first half of the "on" cycle of the ion beam or it can be on during the

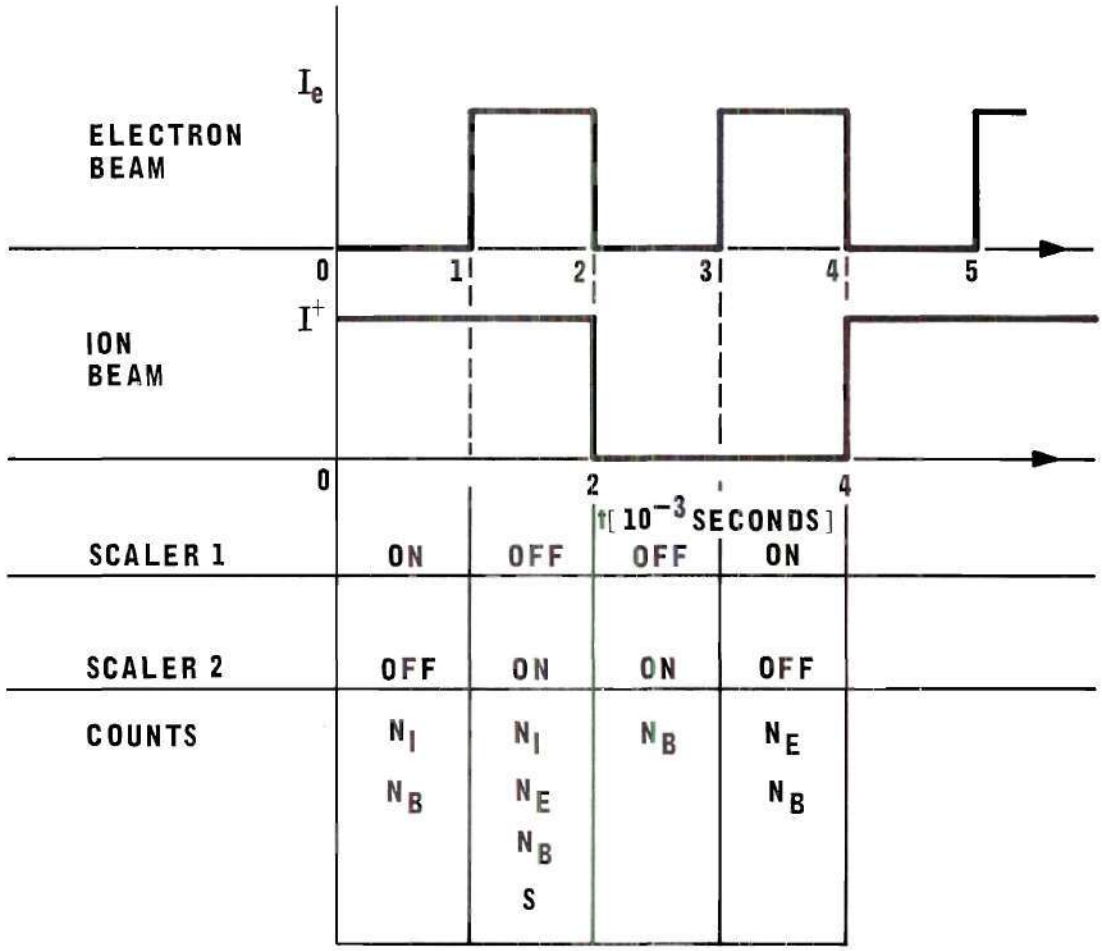

N_I – NOISE COUNT RATE FROM ION BEAM

N_E – NOISE COUNT RATE FROM ELECTRON BEAM

N_B – NOISE COUNT RATE FROM BACKGROUND

S — SIGNAL COUNT RATE

SCALER 1 = $N_I + N_E + 2N_B$

SCALER 2 = $S + N_I + N_E + 2N_B$

Figure 9. Schematic Diagram of Beam Pulsing Sequence.

second half. This phase parameter on the electron beam was alternated throughout the experiment so that any asymmetry in the ion beam was averaged out. With this arrangement, the signal-plus-noise scaler is on when both beams are on or both beams off; the noise scaler is on when only one beam is on.

The principal requirements of the pulsing apparatus are that the pulses have 50 per cent duty cycles, stable pulse widths which are variable from one to ten milliseconds, and rise times of the order of 10^{-3} times the pulse width. These specifications plus the requirement of having both beams switch simultaneously are met with the pulsing apparatus shown in Figure 10. The ion beam was modulated at the horizontal deflection plates rather than the extraction plate of the ion source because of the high leakage current that occurred at the extraction plate due to barium deposited on the insulators.

As shown in Figures 9 and 10, scaler 1 registers the noise while scaler 2 registers the signal plus noise. The difference between the two scalers is therefore the signal, S, within the statistics of the counting process. By counting for a length of time T, scaler 1 has a total count C_{1i} and scaler 2 has C_{2i}. The difference in the two total counts gives a sample of the signal, S_i, where

$$S_i = C_{2i} - C_{1i} . \tag{17}$$

From n such counting periods the mean value of S_i is given by

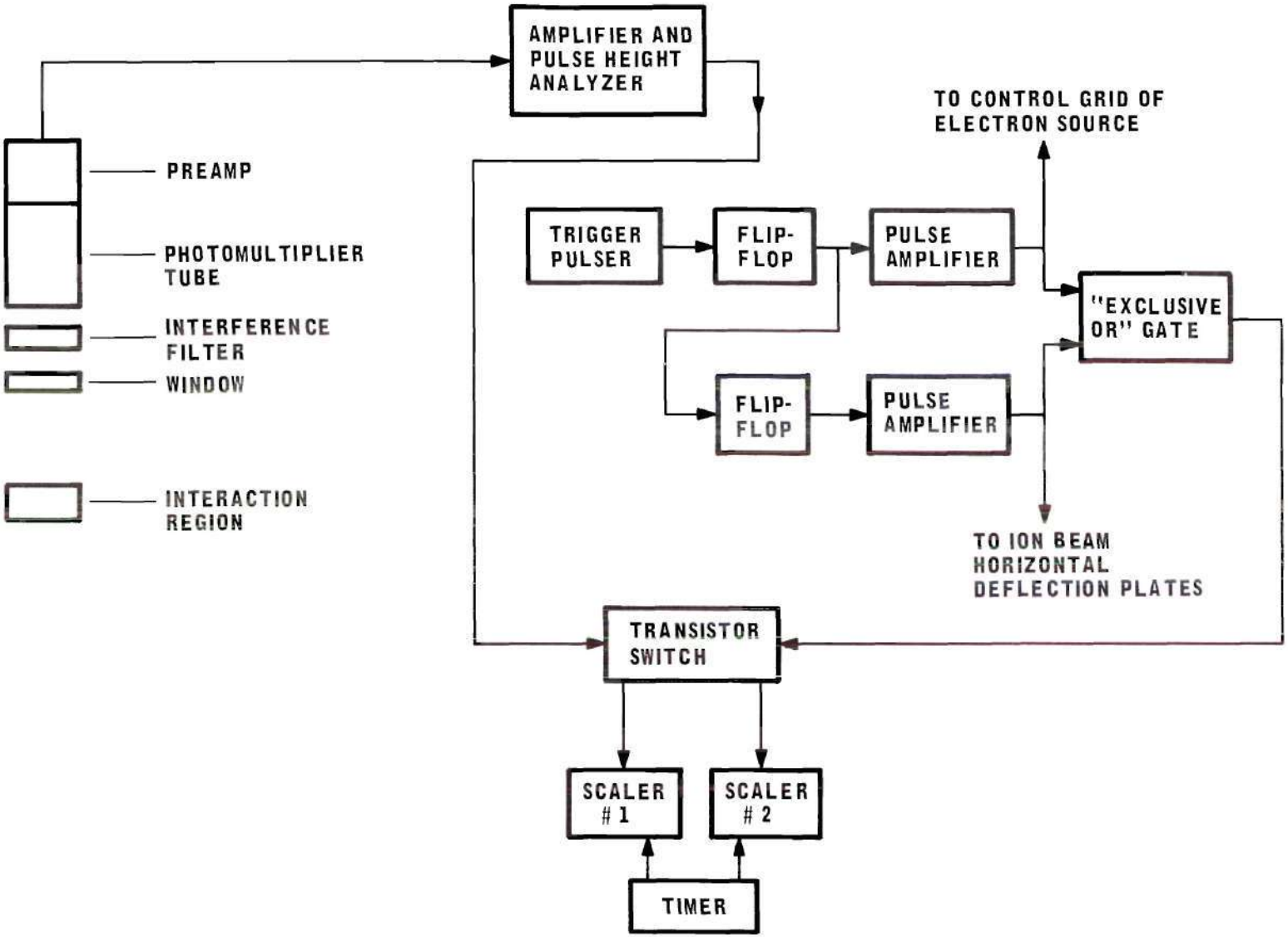

Figure 10. Block Diagram of Pulse Counting and Beam Modulating Equipment.

$$S_n = \frac{1}{n} \sum_{i=1}^{n} S_i \tag{18}$$

and the variance of the samples is

$$\overline{(S_i - S_m)^2} = \frac{1}{n-1} \sum_{i=1}^{n} (S_i - S_m)^2. \tag{19}$$

The average number of counts in both scalers over the n periods is

$$(C_1 + C_2) = \frac{1}{n} \sum_{i=1}^{n} (C_{1i} + C_{2i}). \tag{20}$$

Assuming the signal and noise can be represented as a Poisson sequence of impulses,[30] the theoretical variance in determining S is given by

$$\overline{(S - S_m)^2} = (C_1 + C_2). \tag{21}$$

Since $(C_1 + C_2)$ and S are proportional to T, the ratio of the standard deviation to the signal is proportional to $T^{-1/2}$. Theoretically, by choosing T large enough, the relative scatter in the data may be reduced to an arbitrarily small value. Practically, experimental parameters other than the Poisson statistics enter into the scatter in the data, so reducing the theoretical scatter beyond a certain point becomes meaningless; however, these statistics do apply over short periods of time and provide a meaningful guide for determining T.

Linear Polarizer

The polarization fraction was determined by orienting the axis of a linear polarizer first parallel to the electron beam and then perpendicular to the electron beam as discussed in Chapter II. A Bausch & Lomb type HN 32 linear polarizer with a luminous transmittance of 32 per cent and an extinction transmittance of about 0.005 per cent (two filters, axes crossed, transmit about 0.005 per cent) was used in this experiment. To perform the measurement, the polarizer was placed in the light-tight slide just below the interference filter which had to be removed to rotate the axis of the polarizer.

CHAPTER IV

EXPERIMENTAL PROCEDURES AND RESULTS

The theory for the experiment has been presented in Chapter II while the experimental apparatus and a method for extracting the signal from the various types of noise have been discussed in Chapter III. The experimental procedures and a demonstration that the apparatus performs in a manner consistent with the theory for the experiment are presented in this chapter along with a discussion of the possible sources of error that are not implicit in the theory of the experiment. As indicated in Chapter II, the experimental procedures are divided into the following four groups:

1. Measurement of the relative emission cross section,
2. Measurement of the electron energy distribution,
3. Evaluation of the polarization fraction, and
4. Estimation of the photon detection probability.

Relative Emission Cross Section

The relative emission cross section in terms of the experimental parameters is given by

$$\sigma_{em}^{R} = \frac{S\,F}{I_i\,I_e}\,\frac{e^2\,V_i\,V_e}{(V_i^{\,2} + V_e^{\,2})^{1/2}} \simeq \frac{S\,F}{I_i\,I_e}\,e^2\,V_i \qquad (22)$$

where S is the signal in photons per second, F is the form factor, I_i

and I_e are the ion beam and electron beam currents, e is the electronic charge, and V_i and V_e are the velocities of the ion and electron beams. The beam currents and velocities were straightforwardly determined with the apparatus described in the preceding chapter. After choosing a particular value for the currents and velocities, the form factor was measured using the slit scanner in the differential mode. Before the signal was measured, a counting period was established using the statistical criterion of the preceding chapter. For the majority of the measurements, T was chosen to be 15 minutes; this period resulted in a nominal relative error of 5 per cent. In the latter stages of the data collection, T was shortened to 5 minutes. After counting for a period of time T, the signal was determined by taking the difference between the signal-plus-noise scaler and the noise scaler as discussed in the preceding chapter. After the phase of the electron beam modulation was changed by 180°, another counting period of length T was made; as mentioned in the previous chapter, the phase change on the electron beam modulation averages out any errors due to asymmetries in the ion beam. After four such counting periods where the phase of the electron beam was alternated between each period, the electron beam was turned off and another count for a period T was determined. With the electron beam back on, four more signal counts similar to the first four were made. After these were completed, the ion beam was turned off and another count for a period T was made. Under proper operating conditions, the signal from the counting periods where the beams were off should be zero within the statistics of the counting process; these "beam off" conditions provided a running check on the symmetry of the

pulsing apparatus. Over the entire data collection period, the "signal" from the "beam off" operating conditions averaged to zero with no systematic deviation from zero.

From these eight periods of length T came eight sample values of the signal and eight sample values of the relative emission cross section. One data point for a given set of operating conditions and parameters is the average of a set of eight of these sample values. The raw data and calculated results of a typical measurement are presented in Appendix III. The beam pulsing frequency and the electron cup aperture plate current were recorded with each data run. The data were taken at randomly varied electron energies. In addition, the ion and electron beam intensities were periodically varied to assure that the measured cross sections were independent of these parameters.

Consistency Checks

A number of checks must be made before proper operation of the apparatus is assured. The results of the checks presented here pertain to the performance of the experimental apparatus during those periods in which the experimental results can be considered valid. The most obvious and necessary checks are planned variations of the experimental parameters in Equation (22), which indicates that the signal should be linear with electron beam current and ion beam current and should intercept the origin. Figures 11 and 12 are graphs of signal versus electron beam current and ion beam current which demonstrate the correct functional relationship. The error bars indicate the peak scatter in the experimental data.

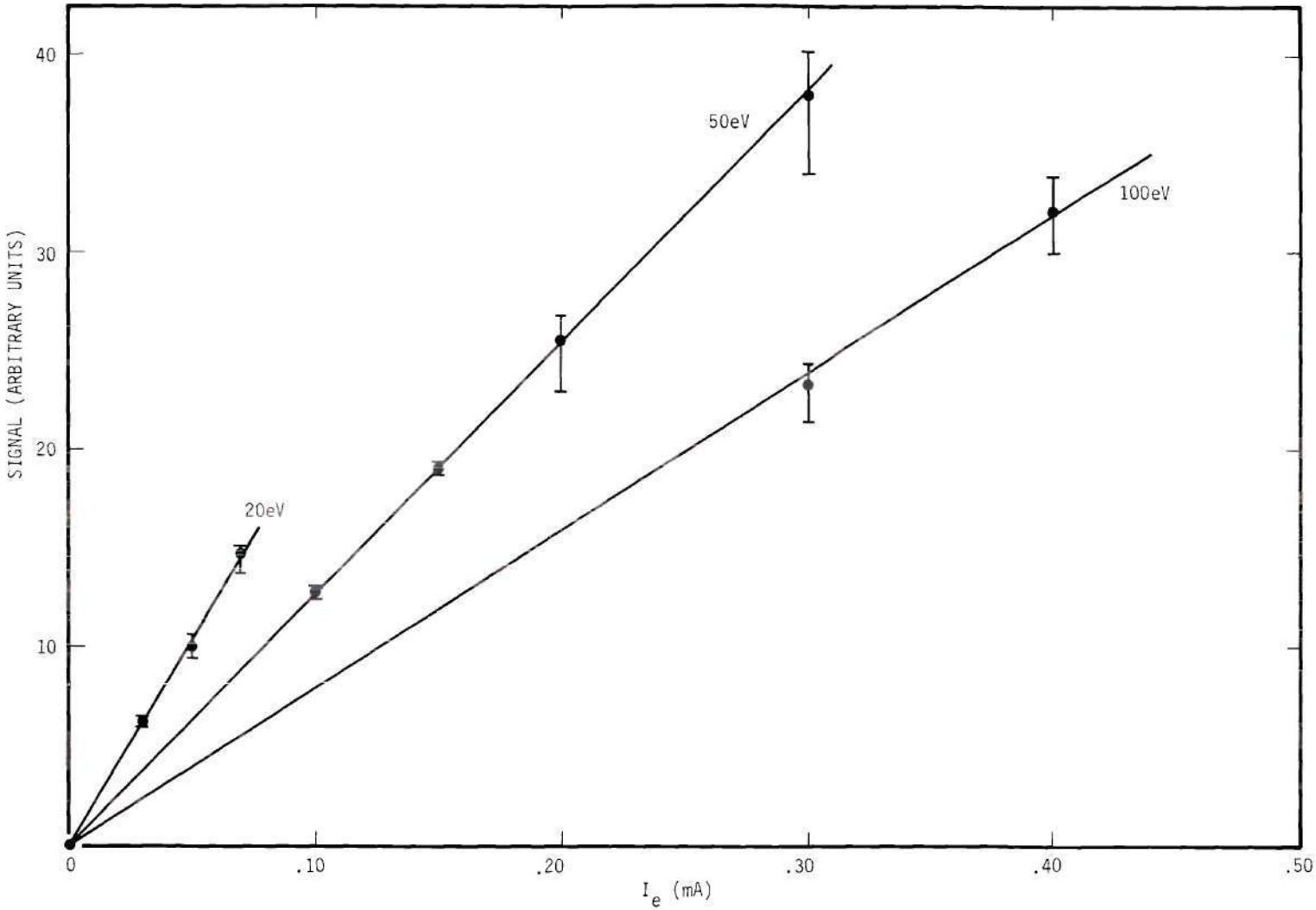

Figure 11. Dependence of Signal upon Electron Beam Current, I_e.

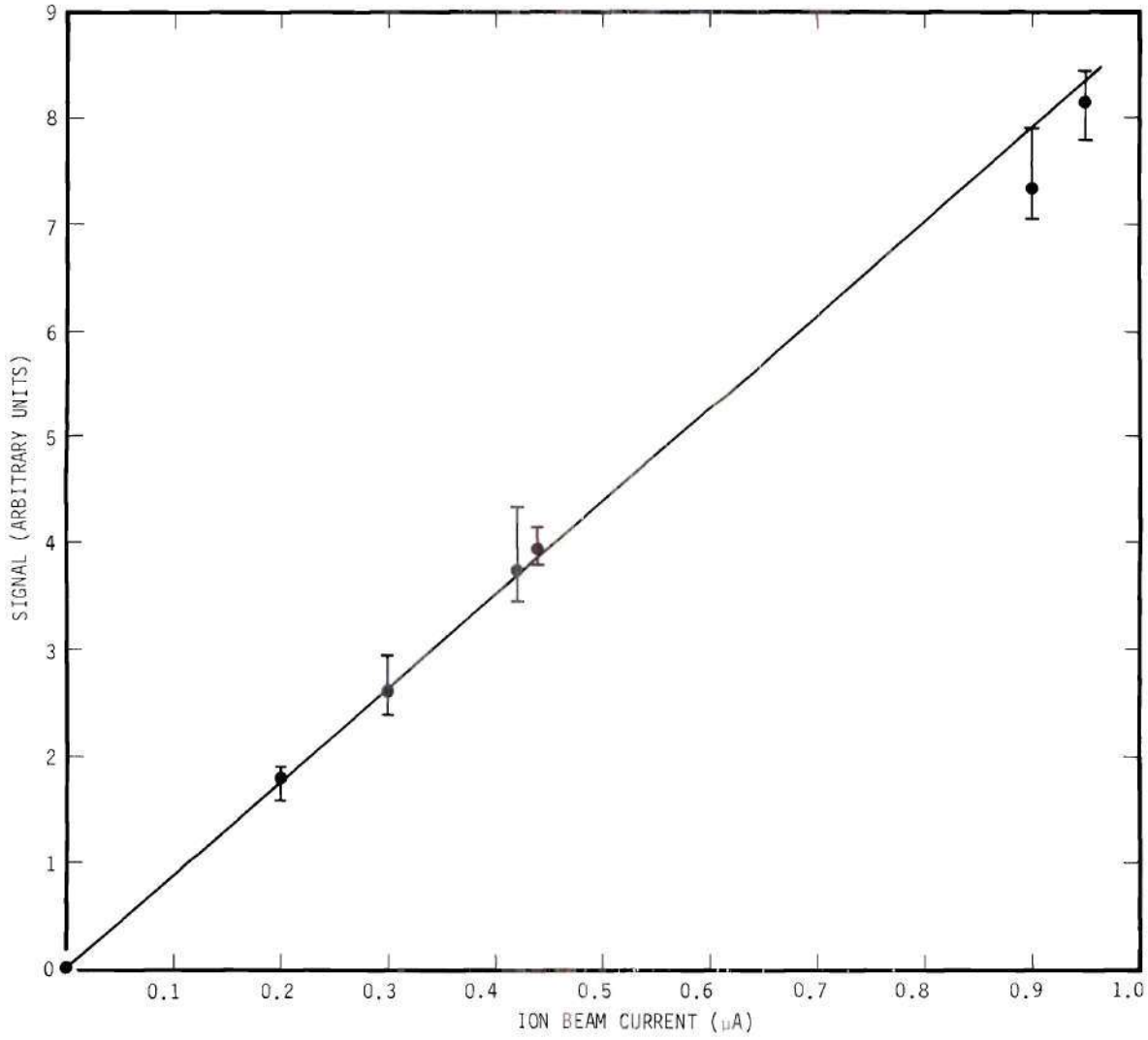

Figure 12. Dependence of Signal upon Ion Beam Current, I_i.

Equation (22) also indicates that the signal should be linear with F^{-1}. Variation of F over a significant range of values in this experiment was not possible; the only variations which did occur were due to incidental changes in the ion beam profile. With these variations, F ranged from 0.95 to 1.20 and showed no systematic effect on the cross section. The electron beam is well contained inside the ion beam and the ion beam is relatively uniform over the region of the electron beam to ensure proper evaluation of F. A typical current distribution of the two beams is shown in Figure 13. With such distributions, the form factor is a measure of the height of the ion beam along the z-axis. (The "hump" at one end of the ion current distribution would tend to make F larger than the height of the ion beam.) If the height of the ion beam is changing as the beam traverses the interaction region, the measured value of F will be incorrect. Such changes in the ion beam can be introduced by passing the beam through an electrostatic lens system which causes the ion beam to either converge or diverge as it passes through the interaction region. To avoid such a possible error in this experiment, the height of the ion beam was collimated to approximately one centimeter rather than focused to this height with an electrostatic lens.

Figure 14 shows the dependence of the measured cross section on ion beam energy and Figure 15 shows the dependence of the cross section on the beam modulation period. The error bars indicate the peak scatter in the experimental data.

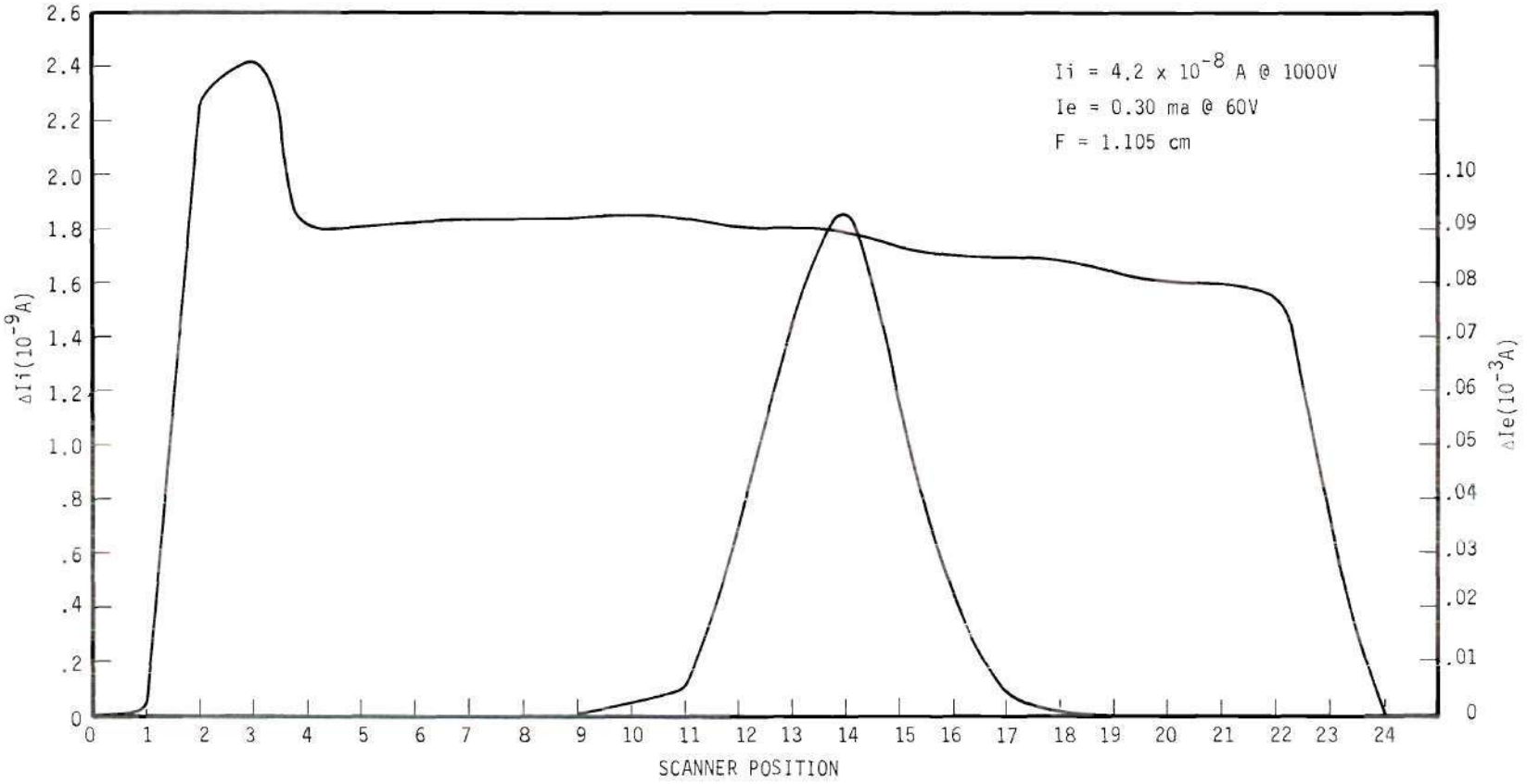

Figure 13. Typical Profile of Ion and Electron Beams. Distance Between Scanner Positions is 0.020 Inch.

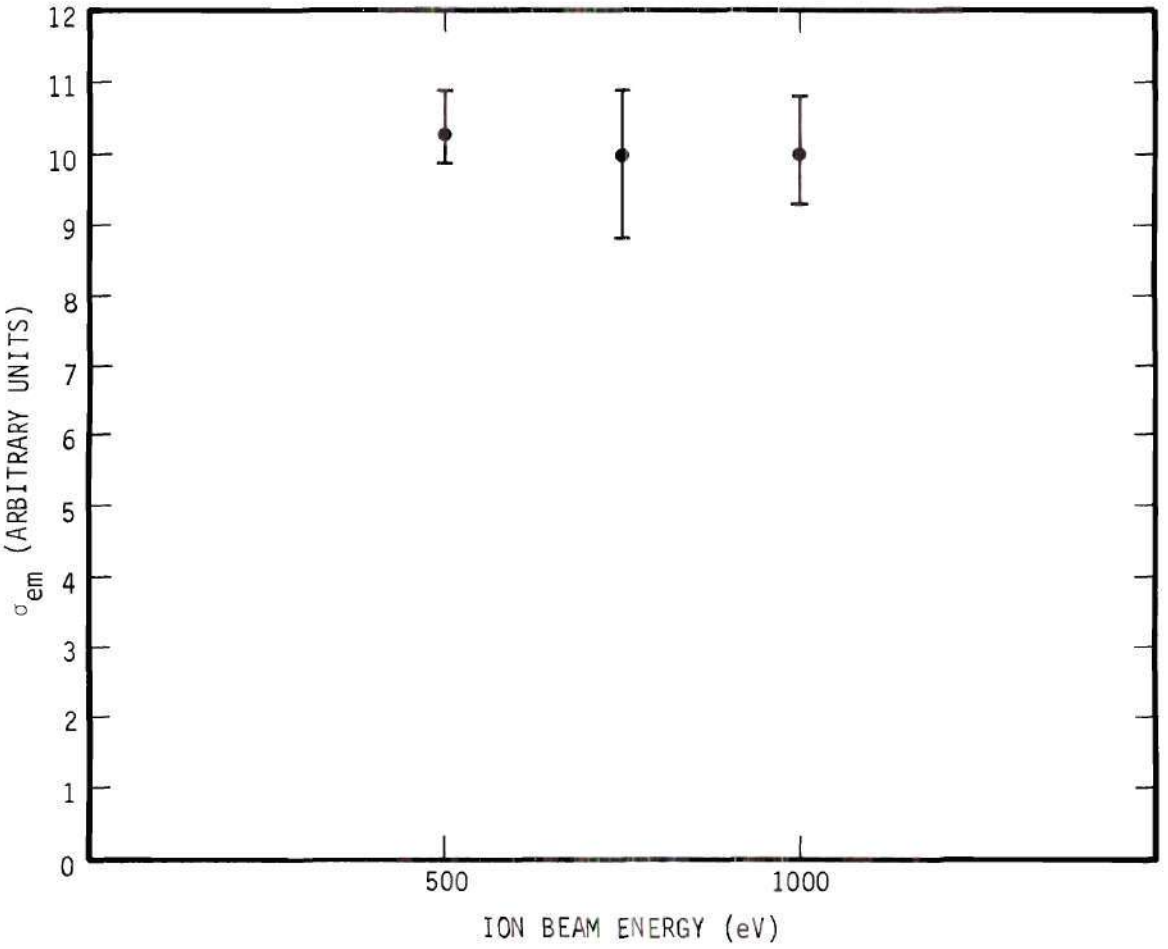

Figure 14. Dependence of Cross Section upon Ion Beam Energy.

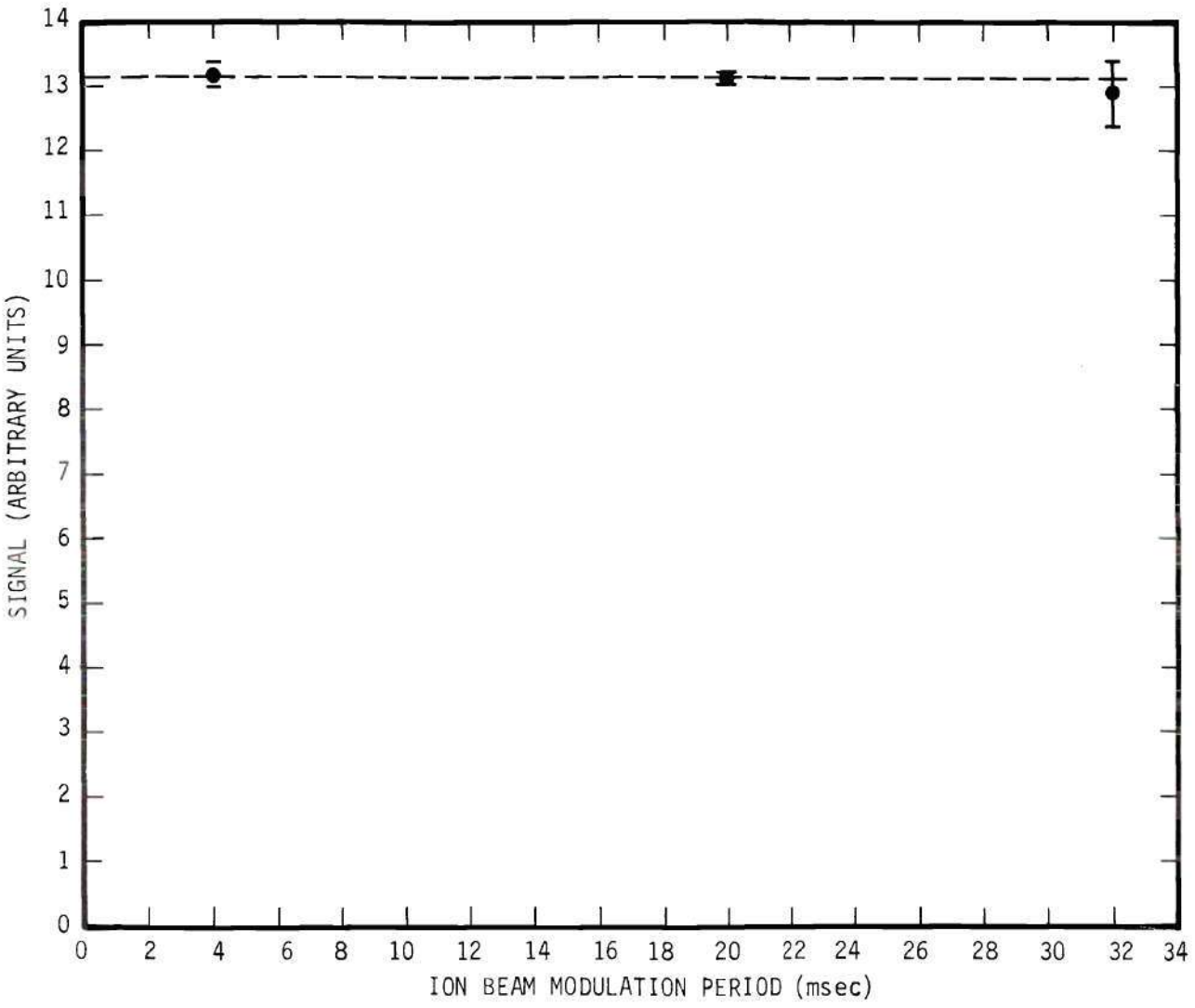

Figure 15. Dependence of Signal upon Ion Beam Pulse Period. The Electron Beam Pulse Period is One-half the Ion Beam Pulse Period.

Possible Sources of Error

This section deals with possible sources of error that can not be detected by the systematic variation of the experimental parameters discussed in the preceding section.

Nonuniformly Activated Electron Source. If the electron source is not uniformly activated or is partially poisoned along the length of its cathode, then this has the effect of changing the collision volume from a uniform distribution of photons to a nonuniform distribution. Since the photon detection probability is possibly not the same for each point in the collision volume, changes in the signal might occur if the collision volume changes. Because of the neutral barium residual gas in the chamber, the electron source cathode was highly activated, especially during the period immediately following bakeout when the pressure remained high and the barium had not been adsorbed by the chamber walls. (Enhanced activation of an oxide cathode in the presence of barium at partial pressures of less than 5×10^{-9} torr has been reported.[31]) The highly activated cathode was observed experimentally by the electron current at the electron cup being nearly equal to the total electron current leaving the cathode, i.e., only that portion of the cathode emitted electrons that was not "shadowed" from the residual barium gas. By turning off the power to the ion source oven and allowing the crucible of barium to cool, the barium partial pressure would decrease and the above "highly activated" conditions on the electron source would disappear.

Under these highly activated conditions, the assumption was made that the electron source cathode was uniformly activated and the electron

cup aperture plate current was recorded for several electron beam currents and energies. These aperture plate currents were established as a "standard" for a uniformly activated electron source cathode. In no case did an electron source produce a beam which gave a lower aperture plate current than that of the standard; however, some electron sources were rejected because they did not meet the specifications of the standard.

Inadvertently, the supposition of a nonuniform photon detection probability over the collision volume was experimentally verified. During a period of three or four days, the apparent cross section increased by 30 per cent and at the same time the aperture plate current increased. Upon disassembly of the apparatus, the electron source cathode was found to be poisoned along half its length. (A poisoned cathode is recognized by its dark gray color.) Installation of a new electron source which met the activation standard resulted in data which agreed with those of earlier measurements.

The fact that the apparent cross section showed an increase rather than a decrease with the above change in the collision volume indicated a misalignment of the lens system. Further investigation showed that the lens was focused at one end of the collision volume, the end where the cathode was not poisoned, instead of being focused at the center of the collision volume. To properly align the lens system, the alignment technique discussed in the previous chapter was devised. The 30 per cent change in the apparent cross section gave an indication of the sensitivity of the detection system to changes in the collision volume; however, in light of the misalignment of the lens system, this sensi-

tivity was probably exaggerated.

Unfortunately, the assumption of a uniform collision volume from an electron source that met the activation standard was never unequivocally proven despite the consistency of the results from several electron sources. However, this consistency of results indicates that the collision volume did not change enough during the measurements to introduce any detectable error in the measured relative cross sections.

In future experiments of this type, a more sensitive technique for checking the uniformity of activation of the electron source cathode would be the use of a slit scanner similar to the one shown in Figure 16.

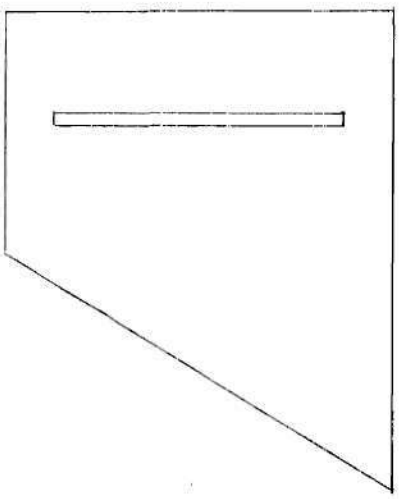

Figure 16. Proposed Electron Beam Scanner

With this scanner, the upper edge and the slit would be used to measure the integral and differential current distributions discussed previously. The wedge-shaped lower edge could be used to give an indication of the

degree of uniformity of cathode activation by measuring an integral of the current distribution along the length of the cathode. However, this measurement would be unnecessary if the photon detection probability were uniform over the collision volume.

Since the ion beam is relatively uniform over its depth of 1 cm, then, in all likelihood, it is uniform over its width of 3 mm. The assumption that the photon detection probability is uniform over the width of the ion beam is probably safe. Hence, the problem discussed above in connection with the electron beam should not arise with the ion beam.

Signal Dependence upon Electron Beam Position. As shown in Appendix II, only the average value of the photon detection probability over the collision volume in the plane of the electron beam maximum enters into the experimental determination of an absolute cross section if

(i) Both beams are uniform over their widths,

(ii) The electron beam is immersed in the ion beam,

(iii) The ion beam is uniform over the extent of the electron beam,

(iv) The electron beam is symmetrical along the Z axis about its maximum which occurs at $z = z_o$,

(v) The height of the electron beam along the Z axis is much less than z_o, the distance of the beam maximum from the limiting aperture of the photon detection system, and

(vi) The average probability that a photon emitted in the z-plane of the collision volume can be represented as

$$n = K_o z_o^2 z^{-2}. \tag{23}$$

The first assumption is discussed in detail in the preceding section. The next four assumptions are very close approximations to the experimental conditions and assumption (vi) should be a good first approximation.

If the position of the electron beam maximum changes when electron sources are changed, an unnecessary systematic scatter in the data will occur. As shown in Appendix II, using assumption (vi), a 3 per cent change in signal will result from shifting the electron beam position 0.040 inch. This indicates the importance of maintaining the same position for the electron beam throughout the experiment. For the present results, the electron beam maximum was maintained at scanner position number 14 as shown in Figure 13 or scanner position number 940 of Table 12 in Appendix III.

Signal Dependence upon Electron Beam Noise. In determining the signal using the pulsing technique described in the previous chapter, the assumption is made that the magnitudes of the noise do not change under the different operating conditions. This assumption was found to be invalid. To discuss the problem, the following terms will be defined.

1. $N_e(I_e,I_i)$ is the noise from the electron beam when both the electron beam and the ion beam are on.

2. $N_e(I_e,0)$ is the noise from the electron beam when only the electron beam is on.

3. $N_i(I_e,I_i)$ is the noise from the ion beam when both the electron beam and the ion beam are on.

4. $N_i(0,I_i)$ is the noise from the ion beam when only the ion beam is on.

Referring to Figure 9, the "noise" scaler or scaler 1 registers $C_1 = 2\,N_b + N_i(0,I_i) + N_e(I_e,0)$ and the "signal plus noise" scaler or scaler 2 registers $C_2 = S + 2\,N_b + N_i(I_e,I_i) + N_e(I_e, I_i)$. In terms of these definitions, the assumptions are:

(a) $N_e(I_e,I_i) = N_e(I_e,0)$ and

(b) $N_i(I_e,I_i) = N_i(0,I_i)$

so that $C_2 - C_1 = S$.

As discussed in the previous chapter, N_e is a function of the electron beam intensity and energy, and the barium partial pressure in the chamber, viz.

$$N_e = \sigma_{ie}\, n_{Ba}\, (I_e/e)\, L\, \eta' \qquad (24)$$

where σ_{ie} is the cross section for ionization with excitation of barium by electron impact, n_{Ba} is the number density of neutral barium, (I_e/e) is the electron beam flux, L is the path length of the electron beam, and η' is the photon detection probability.

The experimental evidence that led to the discovery that assumption (a) was invalid, at least part of the time, was the fact that the cross section increased as the pressure in the chamber decreased. This change in σ would take place only during the first two or three days

after the chamber bakeout routine and was a function of the electron beam energy; at 20 eV there was no change and at 50 eV the increase was less than the increase at 100 eV.

There was never any experimental evidence that assumption (b) was invalid; in fact, on the basis of the explanation of the error in assumption (a), it can be shown that assumption (b) is valid within the statistics of the present experiment. With this knowledge, the difference between scaler 2 and scaler 1 can accurately be given by

$$C_2 - C_1 = S + N_e(I_e,I_i) - N_e(I_e,0). \tag{25}$$

By plotting σ_{em} as a function of (N_e/I_e), the error in assumption (a) may be deduced. Figure 17 shows that σ_{em} decreases as (N_e/I_e) increases. On the basis of Equation (25), this implies that

$$N_e(I_e,I_i) < N_e(I_e,0) \tag{26}$$

for non-zero values of (N_e/I_e).

The ion beam is modulated by modulating the voltage to one of the horizontal deflection plates with 0 - 50 volt pulses. This alternately allows the ion beam to pass through the deflection plates to the interaction region or deflects the ion beam so that it does not pass through the interaction region. While the ion beam is "on" or passing through the interaction region, barium is adsorbed on the surfaces of the deflection plates and the surrounding collimation structures. When the ion beam is "off" or deflected out of the interaction region, barium

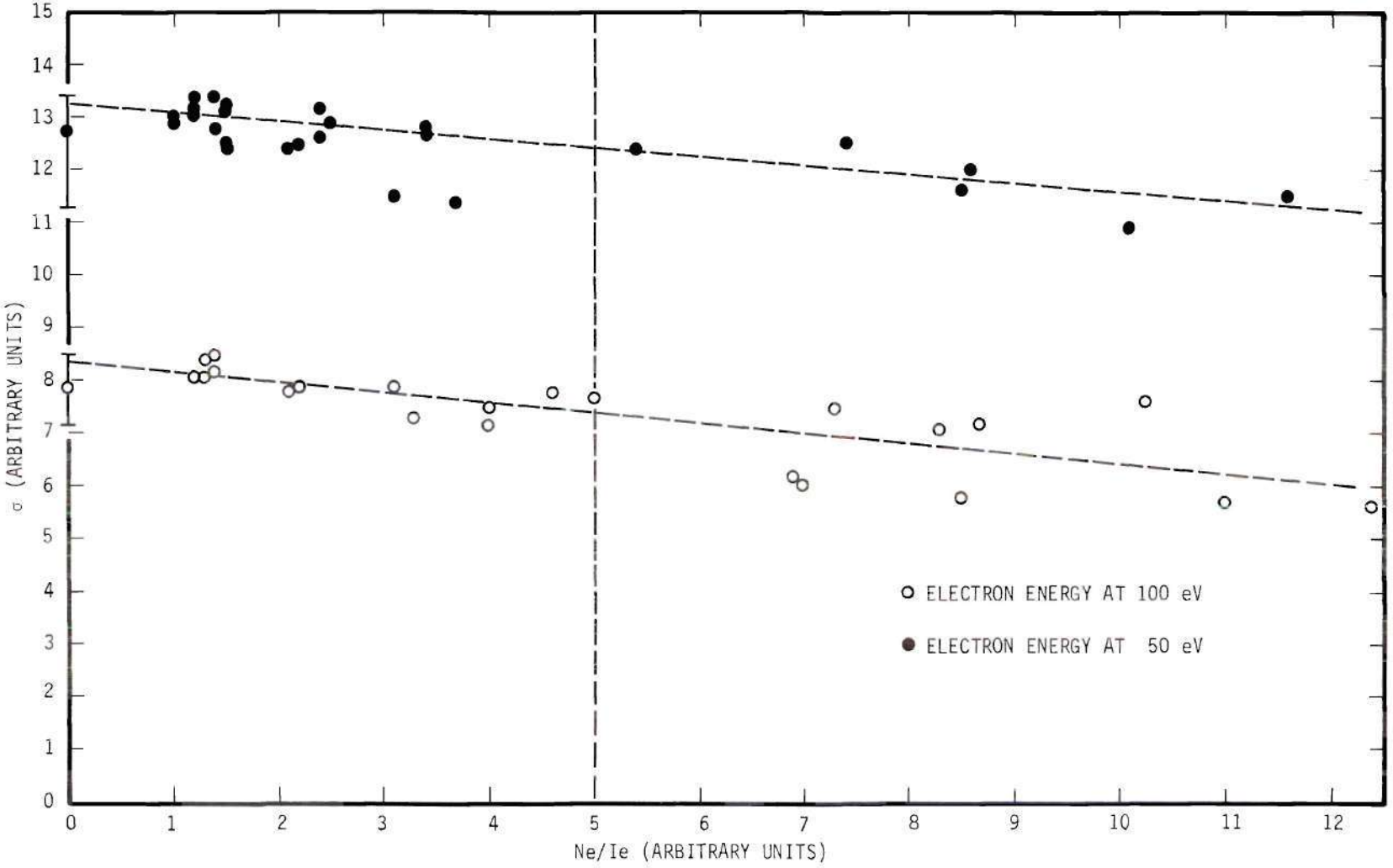

Figure 17. Dependence of Cross Section upon (N_e/I_e).

is dislodged from the surfaces by ion impact causing the barium partial pressure to increase. The amount of barium hitting and sticking to the surfaces during the "on" portion of the cycle will be proportional to the barium partial pressure, and thus the amount of barium coming off the surfaces during the "off" portion of the cycle should also be proportional to the barium partial pressure. Hence, the degree that $N_e(I_e,I_i)$ is less than $N_e(I_e,0)$ should be proportional to the barium partial pressure. This is reflected in Figure 17 by σ_{em} decreasing as (N_e/I_e) increases.

The dependence of the error in σ_{em} on the electron beam energy is explained by the energy dependence of σ_{ie}. At 20 eV $(\sigma_{ie}/\sigma_{em})$ is apparently much less than $(\sigma_{ie}/\sigma_{em})$ at 50 eV which is in turn less than $(\sigma_{ie}/\sigma_{em})$ at 100 eV. Thus at 20 eV no change in σ_{em} within the statistics of the experiment could be detected, while at 50 eV a change in σ_{em} with pressure could be detected which was less than the change at 100 eV.

The fact that there was no apparent dependence of σ_{em} upon pressure at 20 eV is the "experimental evidence" mentioned above that assumption (b) is valid. That is, the pressure dependent error in σ_{em} is a function of electron beam parameters only and not a function of ion beam parameters. Furthermore, since N_i is much smaller in magnitude than N_e at higher pressures, any error in assumption (b) would be much more difficult to detect and, in this experiment, is less than the relative statistical error.

To plot the graph in Figure 17, N_e was determined experimentally by taking the difference between the total count in the "noise" scaler

when both beams were on and the total count in the "noise" scaler when the electron beam was off. Thus (N_e/I_e) was determined for each data point that was measured. By plotting σ_{em} as a function of (N_e/I_e) and extrapolating to (N_e/I_e) equals zero, the "true" value of σ_{em} should be found.

After each reassembly of the apparatus, the 20, 50 and 100 eV data points of the 4554 Å line were remeasured as a check on the experimental apparatus. Because of this procedure, very little data at other energies and none on the 4934 Å line were taken in the higher (N_e/I_e) range. This lack of data at high (N_e/I_e) precluded the use of the extrapolation procedure to determine the "true" σ_{em}. Since no correction can be made on the measured values of σ_{em}, no data are included in the final averages when taken at $(N_e/I_e) > 5$ on the relative scale of Figure 17 and a positive systematic error is added to the final average to allow for a possible increase in the reported value of σ_{em}. The positive systematic error is energy dependent; from 10 to 30 eV there is no additional error and at 100 eV there is a +6 per cent systematic error. Table 3 gives the systematic error as a function of the indicated electron energy. These values of error were determined on the basis of the extrapolation in Figure 17 where the average of the data taken at $(N_e/I_e) \leq 5$ is shown on the ordinate of the graph along with the peak scatter of the data included in the final average.

A better cooled ion source and improved trapping of the neutral barium in the ion beam would eliminate this pressure dependent error in σ_{em}. The improved trapping could be achieved by cooling the back plate of the electrostatic analyzer.

Table 3. Systematic Error in σ_{em}^{R} Necessary to Account for a Possible Pressure Effect upon Measurements

Indicated Electron Energy (eV)	Systematic Error (%)
10 - 30	0
40	+1
50	+3
60	+3
70	+4
80	+4
90	+5
100	+6

Electron Beam Energy Distribution

The electron beam energy distribution was measured at 20, 50 and 100 eV using the procedure described in the previous chapter. Energy distributions were measured after each reassembly of the apparatus and the measurements were repeated periodically. A typical electron beam energy distribution is shown in Figure 18. The average full-width-half-maximum of the energy distribution is 1.5(±0.5)eV; the energy distribution of the electron beam is, therefore, sufficiently narrow that no deconvolution of the data is necessary. The peak of the energy distribution occurs at a voltage below the indicated electron

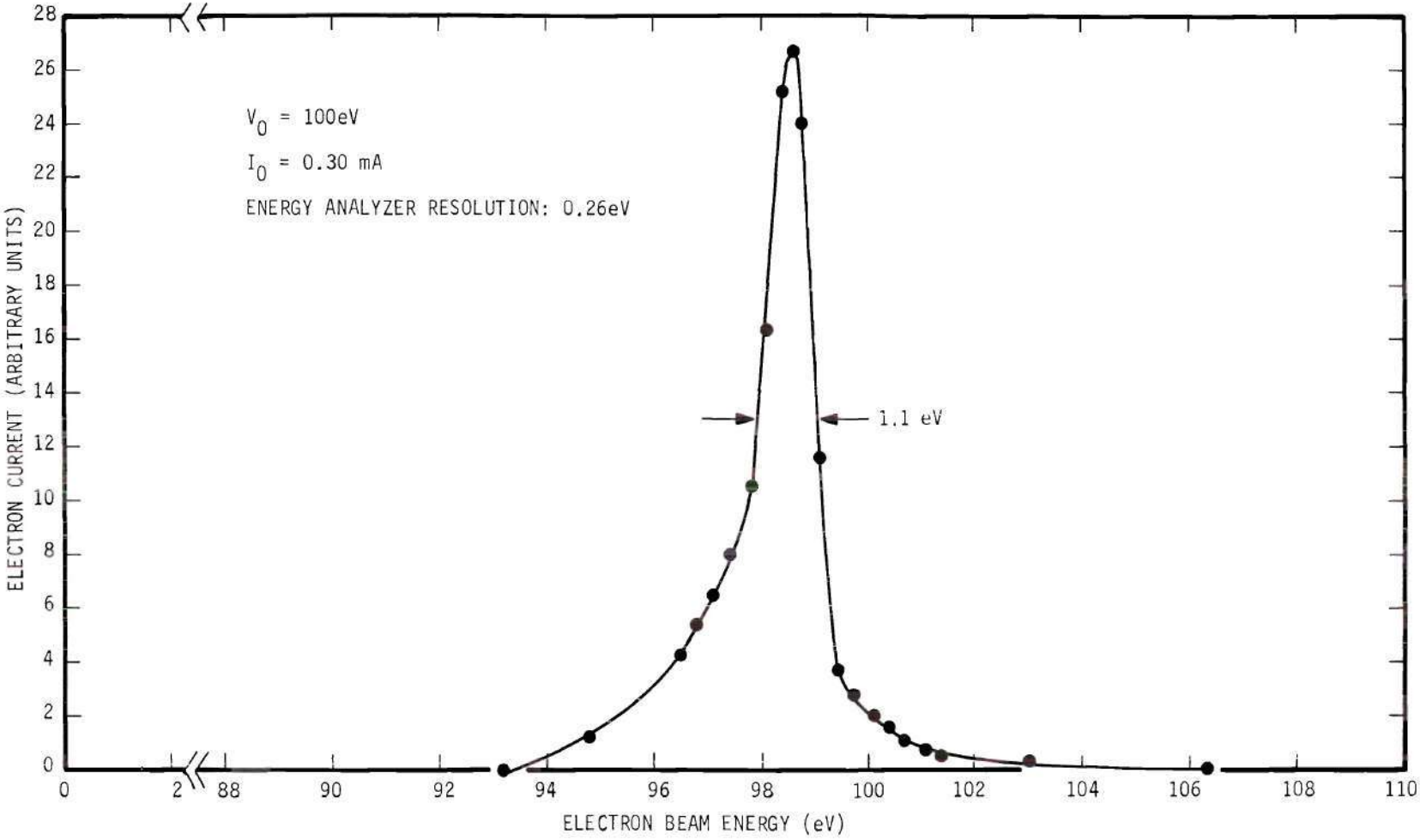

Figure 18. Typical Electron Beam Energy Distribution.

voltage; the average difference in these two voltages is 2(±1) volts. To correct the data for this shift in the indicated electron energy, the actual electron energy was taken to be 2(±1) volts below the indicated value.

Relative Cross Section Data and Errors

The relative cross section data and errors are given in tabular form in Tables 4 and 5 and in graphical form in Figure 19. These data are the experimental data multiplied by a factor of 10^{20}. The random error given in the tables covers over 95 per cent of the experimental data. The standard deviation and the 90 per cent confidence limits[32] are included for comparison with other experimental presentations. As shown in Appendix III, the standard deviation is largely due to the Poisson statistics of the counting process. The systematic error is the sum of all the systematic errors discussed in the previous chapter, presented in Table 6, plus the pressure dependent error given in Table 3. The data presented here were taken over a period of three months while the apparatus was assembled and disassembled seven different times. The data showed no systematic variation other than the systematic pressure dependence over this period of time.

$6^2P^o_{1/2} \rightarrow 6^2S_{1/2}$

INDICATED ELECTRON ENERGY (eV)	ACTUAL ELECTRON ENERGY (eV)	σ_{em}	STANDARD DEVIATION (%)	90% CONFIDENCE LIMITS (%)	RANDOM ERROR(*) (%)	SYSTEMATIC ERROR (%)	TOTAL ERROR (%)
10	8±1	14.0	±24	±15	±30	±6	±36
20	18±1	9.6	±7	±4	±20	±6	±26
30	28±1	7.8	±11	±9	±20	±6	±26
40	38±1	6.8	±5	±3	±20	+7 -6	+27 -26
50	48±1	6.1	±9	±6	±20	+9 -6	+29 -26
60	58±1	5.6	±13	±7	±20	+9 -6	+29 -26
70	68±1	5.1	±5	±4	±16	+10 -6	+26 -22
80	78±1	4.6	±8	±5	±16	+10 -6	+26 -22
90	88±1	4.2	±4	±3	±16	+11 -6	+27 -22
100	98±1	3.9	±10	±5	±16	+12 -6	+28 -22

* THE RANDOM ERROR ENCLOSES ALL DATA POINTS EXCEPT THREE OUT OF A TOTAL OF 93.

Table 4. Relative Emission Cross Section Data and Errors.

$6^2P^o_{3/2} \rightarrow 6^2S_{1/2}$

INDICATED ELECTRON ENERGY (eV)	ACTUAL ELECTRON ENERGY (eV)	σ_{em}	STANDARD DEVIATION (%)	90% CONFIDENCE LIMITS (%)	RANDOM ERROR(*) (%)	SYSTEMATIC ERROR (%)	TOTAL ERROR (%)
10	8±1	27.7	±7	±4	±10	±6	±16
20	18±1	20.3	±4	±2	±10	±6	±16
30	28±1	16.6	±6	±5	±10	±6	±16
40	38±1	14.3	±5	±3	±10	+7 -6	+17 -16
50	48±1	12.8	±5	±2	±10	+9 -6	+19 -16
60	58±1	11.7	±5	±3	±10	+9 -6	+19 -16
70	68±1	10.3	±6	±5	±10	+10 -6	+20 -16
80	78±1	9.7	±5	±4	±10	+10 -6	+20 -16
90	88±1	8.8	±4	±2	±10	+11 -6	+21 -16
100	98±1	7.9	±5	±3	±10	+12 -6	+22 -16

* THE RANDOM ERROR ENCLOSES ALL DATA POINTS EXCEPT THREE OUT OF A TOTAL OF 109.

Table 5. Relative Emission Cross Section Data and Errors.

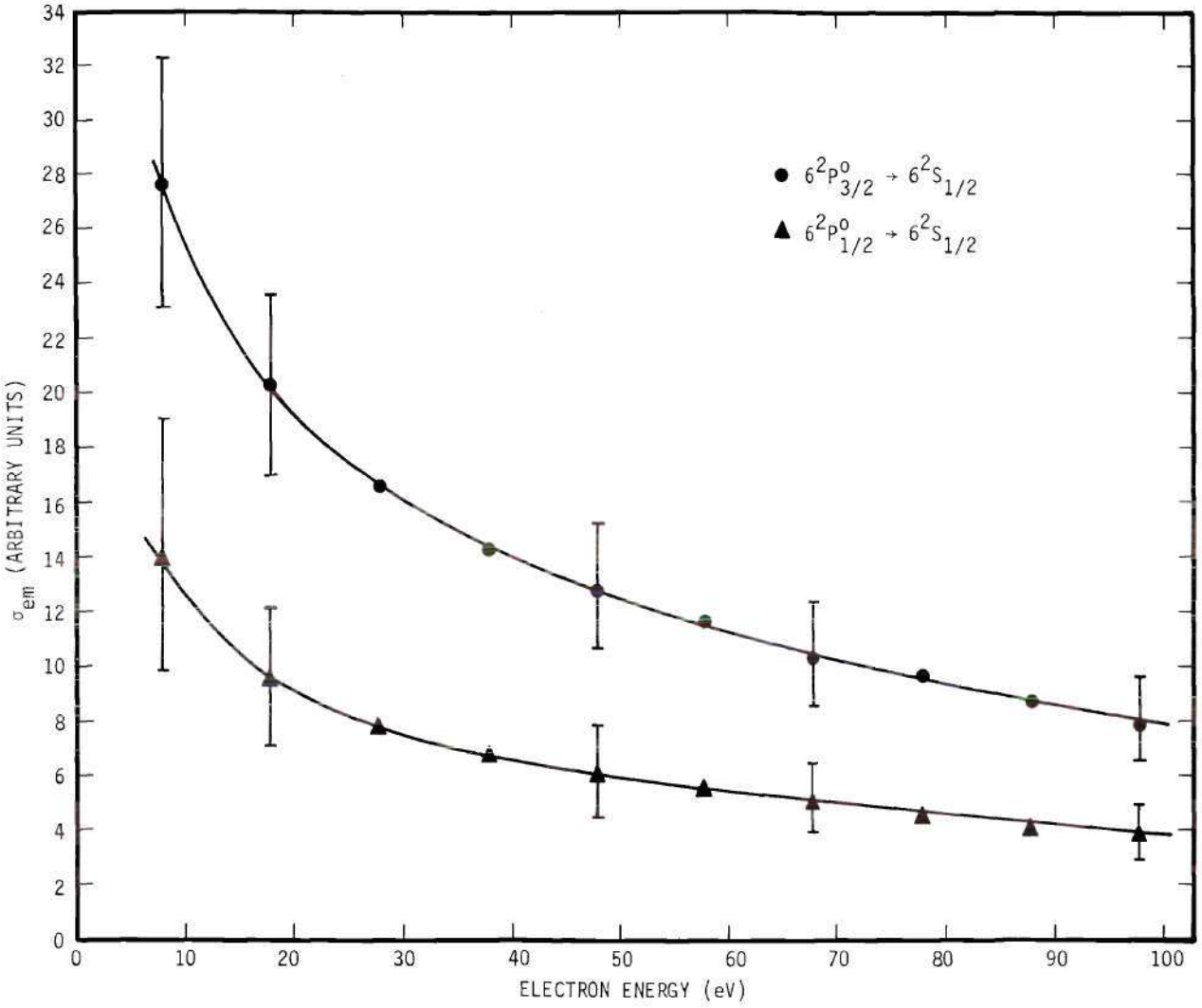

Figure 19. Dependence of Relative Emission Cross Sections upon Electron Energy. Measured Cross Section Multiplied by 10^{20}.

Table 6. Systematic Errors in the Relative Emission Cross Section

Experimental Parameter	Systematic Error %
F	±2
I_e	±2
I_i	±2
V_i	±0.50

Polarization Fraction

With the addition of the polarizing film, the procedure for measuring the polarization fraction was similar to the procedure for measuring the relative emission cross section. From eight five-minute counting periods, an average value of $\phi_{\parallel}$ was determined when the axis of the polarizer was aligned parallel to the electron beam, and similarly, from eight five-minute counting periods, an average value of $\phi_{\perp}$ was determined when the axis of the polarizer was perpendicular to the electron beam. The polarization fraction is given by

$$P = \frac{\phi_{\parallel} - \phi_{\perp}}{\phi_{\parallel} + \phi_{\perp}} . \qquad (27)$$

This procedure was repeated eight times at 20, 50 and 100 eV indicated electron energies for both the 4934 Å line and the 4554 Å line to determine an average value of P at each of these energies. The results of

these measurements are presented in Table 7 along with the maximum scatter in the experimental data.

Table 7. Polarization Fraction

Indicated Electron Energy (eV)	Polarization Fraction (%)	Maximum Experimental Scatter
$6^2P^o_{3/2} \rightarrow 6^2S_{1/2}$		
20	+3	±12
50	-3	± 5
100	-8	± 7
$6^2P^o_{1/2} \rightarrow 6^2S_{1/2}$		
20	-3	±28
50	-3	± 6
100	0	± 8

A smooth curve drawn through a graphical presentation of these data and extrapolated to 10 eV indicates that the magnitude of the polarization is less than 15 per cent; this value also encloses most of the experimental scatter. As indicated by Equation (10) in Chapter II, a 15 per cent value for the polarization changes the measured cross section by 5 per cent. Because of the small magnitude of the polarization data

and the accompanying large experimental scatter, no attempt was made to correct the relative cross section for the polarization fraction. Instead, a ±5 per cent uncertainty was added to the relative emission cross section to allow for a possible ±15 per cent polarization fraction.

Estimate of Photon Detection Probability

This experiment was initially designed without a lens system. The cross section for the 4554 Å line was measured at several electron energies using this design. However, when attempts to measure the cross section for the 4934 Å line were made, the scatter in the data was too high for satisfactory results because of a lower signal and a higher background noise. To overcome this problem, the present lens system was designed and installed.

With the no-lens-system, the photocathode was collimated so that each point on the cathode could "see" every point in the collision volume. Hence, estimating the total solid angle that the photocathode subtended about the collision volume was a straightforward procedure. The exposed area of the photocathode was 5/8 square inches at a distance of 9-13/16 inches from the center of the collision volume. The fractional area that the cathode subtended was 5.2×10^{-4} with an estimated error of ±5 per cent. An estimate of the transmission efficiency of the interference filters and the windows on the vacuum chamber and in the cooling unit, and the quantum efficiency of the photomultiplier tube was available from the manufacturer of each item. These values along with their estimated errors are given in Table 8.

Table 8. Estimate of Photon Detection Probability

	λ = 4554 Å	λ = 4934 Å	Estimated Error Per Cent
Fractional Area of No-Lens System	5.2×10^{-4}	5.2×10^{-4}	± 5
Transmission of Window on Vacuum Chamber	0.90	0.90	± 5
Transmission of Windows in PM Tube Cooler	0.82	0.82	± 5
Quantum Efficiency of EMI 9584 S	0.07	0.065	±10
Transmission of Interference Filters	0.64	0.63	± 5
Approximate Overall Detection Probability Without Lens System	1.72×10^{-5}	1.57×10^{-5}	±30
Increase in Signal with Lens System Installed	8.2	8.2	±10
Approximate Overall Detection Probability With Lens System	1.4×10^{-4}	1.3×10^{-4}	±40

After the lens system was installed, the signal increased by a factor of 8.2 giving an estimated overall detection probability of 1.4×10^{-4} at λ = 4554 Å and 1.3×10^{-4} at λ = 4934 Å. The estimated systematic error on these values is ±40 per cent which represents a sum

of the estimated systematic errors listed in Table 8.

Estimated Absolute Cross Sections

The relative emission cross sections given in Tables 4 and 5 are multiplied by a factor of 10^{+20}. Taking this factor into consideration along with the estimated photon detection probability as shown by Equation (10) gives the estimated absolute cross sections. These data are presented in Tables 9 and 10. As discussed previously, a ±5 per cent error is added to the estimated absolute cross sections to allow for a possible ±15 per cent polarization fraction.

Table 9. Estimated Absolute Emission Cross Section for Excitation of the $6^2P^o_{3/2} \rightarrow 6^2S_{1/2}$ Transition in Ba^+ Ions by Electron Impact

Actual Electron Energy (eV)	σ_{em} (10^{-16} cm^2)	Total Error in Relative Cross Section (%)	Total Error in Estimated Absolute Cross Section (%) (See Note)
8	19.8	±16	±61
18	14.5	±16	±61
28	11.9	±16	±61
38	10.2	+17 -16	+62 -61
48	9.1	+19 -16	+64 -61
58	8.4	+19 -16	+64 -61
68	7.4	+20 -16	+65 -61
78	6.9	+20 -16	+65 -61
88	6.3	+21 -16	+66 -61
98	5.6	+22 -16	+67 -61

NOTE: The total error in the estimated absolute cross section is the sum of the total error in the relative cross section plus the ±5 per cent error due to polarization plus the ±40 per cent error in the estimated photon detection efficiency.

Table 10. Estimated Absolute Emission Cross Section for Excitation of the $6^2P^o_{1/2} \rightarrow 6^2S_{1/2}$ Transition in Ba^+ Ions by Electron Impact

Actual Electron Energy (eV)	σ_{em} (10^{-16} cm^2)	Total Error in Relative Cross Section (%)	Total Error in Estimated Absolute Cross Section (%) (See Note)
8	10.8	±36	±81
18	7.4	±26	±71
28	6.0	±26	±71
38	5.2	+27 -26	+72 -71
48	4.7	+29 -26	+74 -71
58	4.3	+29 -26	+74 -71
68	3.9	+26 -22	+71 -67
78	3.5	+26 -22	+71 -67
88	3.2	+27 -22	+72 -67
98	3.0	+28 -22	+73 -67

NOTE: The total error in the estimated absolute cross section is the sum of the total error in the relative cross section plus the ±5 per cent error due to polarization plus the ±40 per cent error in the estimated photon detection efficiency.

CHAPTER V

COMPARISONS WITH THEORY

The only quantum mechanical thecry presently available on the excitation of Ba^+ by electron impact is the general treatment of excitation developed by Bethe.[19] Using hydrogen-like wave functions and the Born approximation he has shown that at high electron energies the cross section for electron excitation of electric dipole transitions is given by

$$\sigma_{ex}(i \rightarrow j) = \frac{4\pi\, a_o^2\, R^2\, f_{ij}}{(E_j - E_i)\, E} \ln\left[\frac{C\, E}{E_j - E_i}\right] \qquad (28)$$

where a_o is the radius of the first Bohr orbit of the hydrogen atom, R is the rydberg constant, E_i and E_j are the energies of the lower and upper levels, f_{ij} is the optical oscillator strength for the transition, E is the energy of the projectile electron, and C is a constant which must be evaluated for each atom or ion. In principle, f_{ij} and C can be determined but lack of accurate wave functions prevents this for most atoms or ions. Even without knowing these constants, the energy dependence of σ_{ex} at high electron energies is predicted to be

$$\sigma_{ex} = \frac{A}{E} + \frac{B}{E} \ln (E) \qquad (29)$$

where A and B are constants. That the relative experimental data follow

this energy dependence at high electron energies is shown in Figure 20.

Seaton[20] has attempted to generalize Bethe's results to lower electron energies by introducing an empirical factor, $\bar{g}$, so that

$$\sigma_{ex}(i \to j) = \frac{8\pi^2 a_o^2 R^2 f_{ij}}{3^{1/2}(E_j - E_i)\, E}\, \bar{g} \tag{30}$$

where, at high electron energies,

$$\bar{g} = \frac{3^{1/2}}{2\pi} \ln\left[\frac{E}{E_j - E_i}\right]. \tag{31}$$

At low and intermediate energies $\bar{g}$ is empirically evaluated with calculated and measured excitation cross sections. This empirical factor is tabulated by Van Regemorter[33] and also by Allen.[34] For strong allowed transitions, the strong coupling effects reduce the cross section by a factor of the order of two near threshold.[18,33] At high energies the accuracy may be expected to decrease as increasing departure from the one-electron atom is introduced. Using the experimental values of the oscillator strengths for Ba^+ obtained by Gallagher,[2] the cross section for the excitation of the 6^2P levels of Ba^+ has been calculated using Equation (30). The results are presented in Figure 21.

The only other available theory for comparison with experimental results is the semi-classical collision theory of Gryzinski.[21] Calculations based on this theory, though directly applicable only to neutral targets, should approach the cross section for excitation of the ion at high electron energies where the coulomb field of the ion becomes

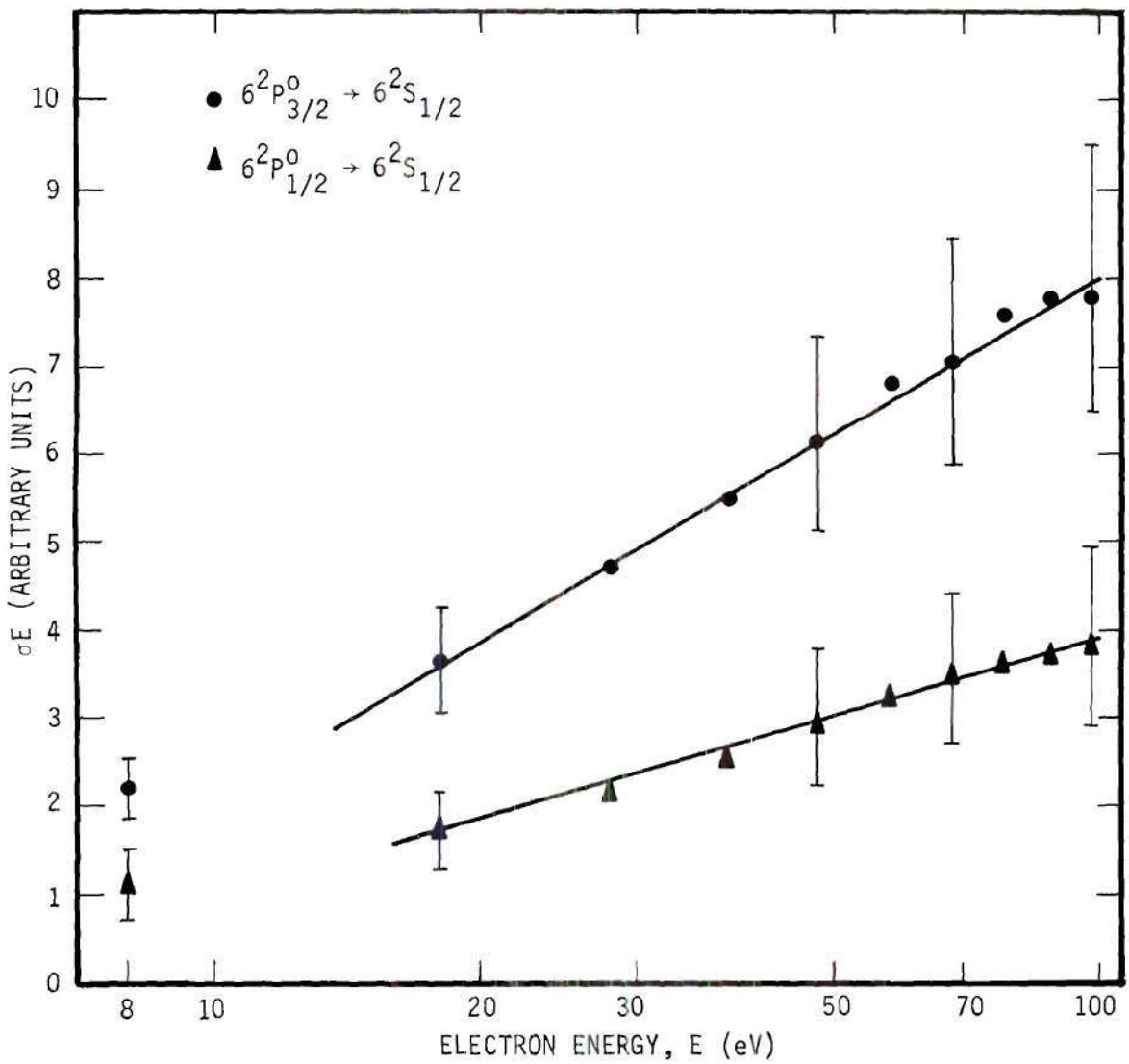

Figure 20. Relative Emission Cross Section Times Electron Energy versus Electron Energy, Demonstrating Form of Equation (29).

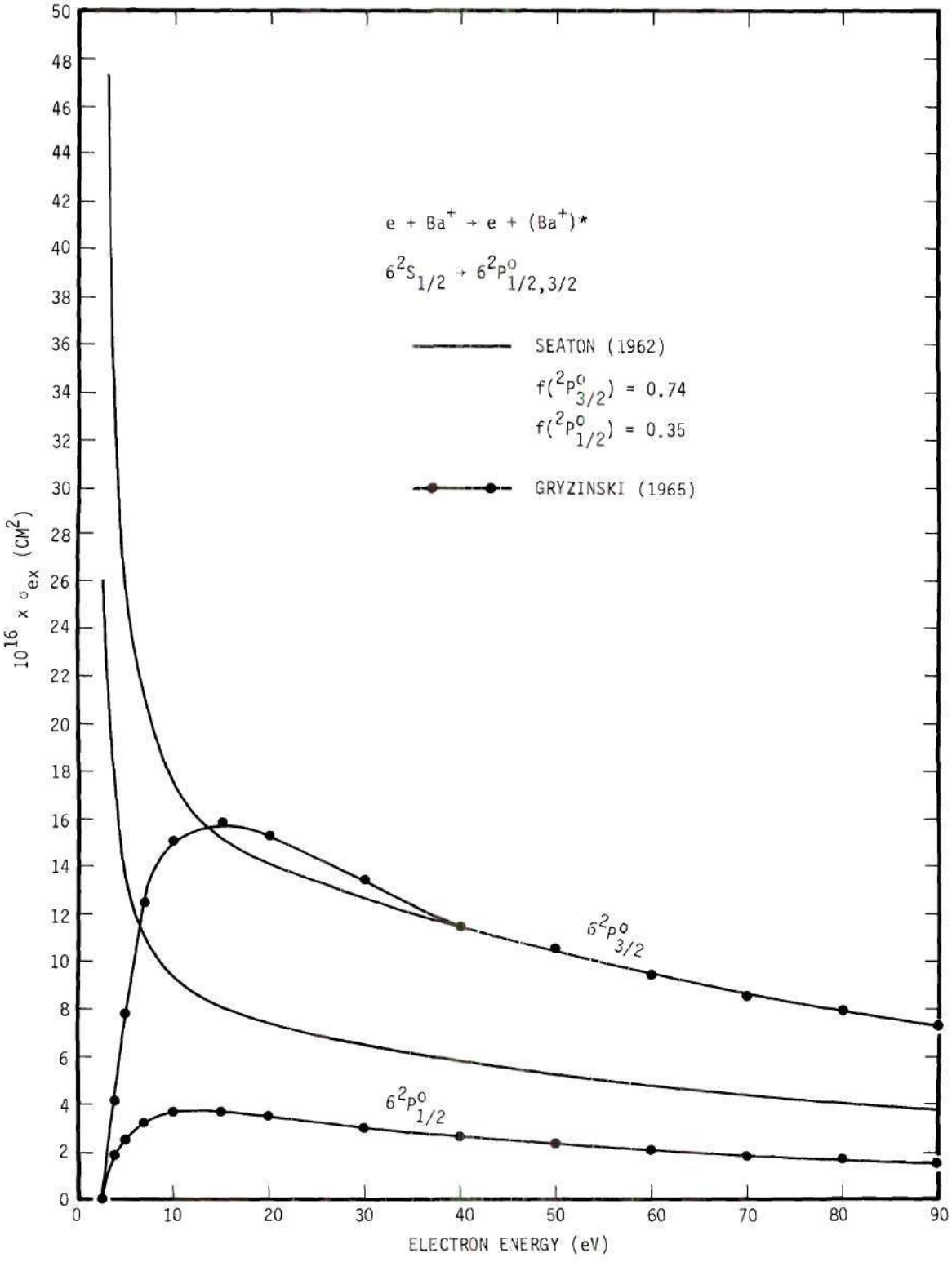

Figure 21. Theoretical Excitation Cross Sections versus Electron Energy.

negligible. Results of such a calculation are presented in Figure 21. Notice that the ratio of the two cross sections at high electron energies is about 4.5, whereas, the ratio based on Seaton's theory is about two. When the energy difference between the two 6^2P levels is small compared to the electron energy, the ratio of the two cross sections should vary approximately as the ratio of the statistical weights of the two levels which, in this case, is two. Thus, in this respect, the calculations based on the theory of Gryzinski are incorrect although yielding results that are the same order of magnitude as those from Equation (30).

To compare the experimental results with the theoretical predictions of the excitation cross section, the branching ratios and cascading effects must be included as indicated by Equation (4) in Chapter II. The branching ratios for the $6^2P \rightarrow 5^2D$ transitions and the $6^2P \rightarrow 6^2S$ transitions have been experimentally determined by Gallagher[2] to be 0.26 and 0.74 within an accuracy of ±10 per cent. The only information on the cascading contribution to the emission cross section is that which can be inferred from the study of excitation of Cs, which is isoelectronic with Ba^+. In their experimental investigation of the excitation of Cs by electron impact, Zapesochnyi and Shimon[35] found that the cascade contribution to the resonance line emission cross section was approximately 10 per cent. Assuming the resonance line emission cross section of Ba^+ contains the same relative cascading effects and using the above values of the branching ratios, the theoretical values of the excitation cross section are converted to an emission cross section. In Figure 21, the comparison is made between the results from

the Seaton formula and the estimated absolute cross sections given in Tables 9 and 10. The agreement between experiment and theory is remarkable considering the 60 to 80 per cent error brackets on the experimental data and the 20 per cent error brackets on the theoretical curve due to the experimental determination of the branching ratios, oscillator strengths and cascading.

The general theory on polarization by Percival and Seaton[22] predicts a polarization value of 53 per cent at threshold with a high energy limit of -37 per cent for the Ba^+ $6^2P^o_{3/2} \rightarrow 6^2S_{1/2}$ transition and zero polarization for the $6^2P^o_{1/2} \rightarrow 6^2S_{1/2}$ transition. Qualitatively, the experimental data agree with these predictions; the data for the $6^2P^o_{3/2} \rightarrow 6^2S_{1/2}$ transition are positive at low energies and decrease to negative values at high energies, and the data for the $6^2P^o_{1/2} \rightarrow 6^2S_{1/2}$ transition are zero within the experimental scatter.

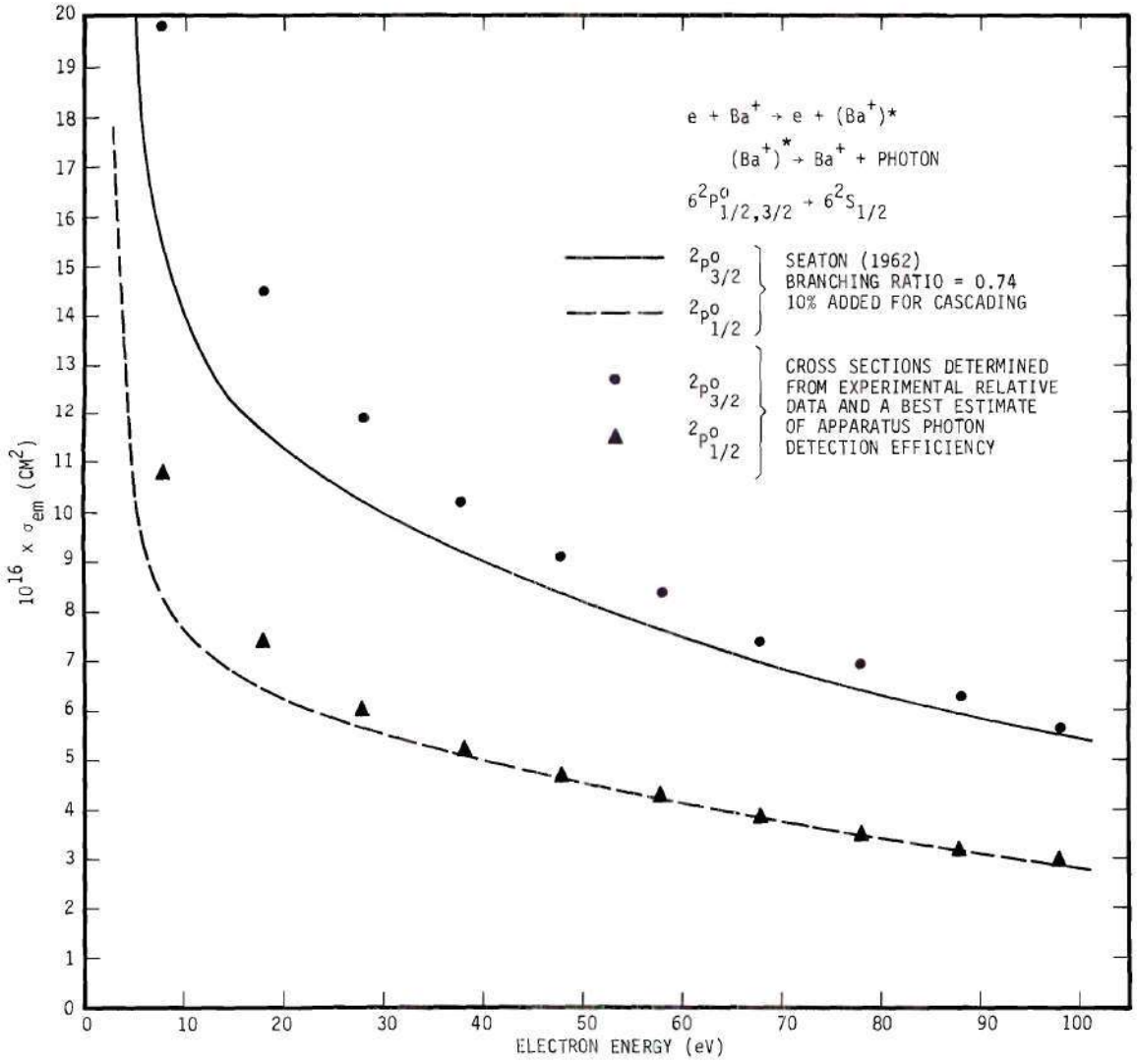

Figure 22. Comparisons Between Estimated Absolute Emission Cross Sections and Theoretical Absolute Emission Cross Sections.

CHAPTER VI

CONCLUSIONS

A crossed beam technique has been developed for measuring the emission cross section for the excitation of electric dipole transitions in ions by electron impact. The experimental method involves crossing modulated ion and electron beams in a well defined collision volume. A portion of the radiation from the excited ions is detected at an angle of 90° to the plane of the two beams by direct observation of the collision volume with a photomultiplier tube. The selection of a single emission line is accomplished with an interference filter. The total flux of radiation from the collision volume for a particular transition can be determined with a knowledge of the photon detection probability of the apparatus. The possibility of an anisotropic angular distribution of radiation from the collision volume is evaluated by measuring the polarization fraction. The emission cross section can be determined from the ion and electron beam currents, current density distributions and energies, and the total radiation flux.

The technique has been used to measure the relative emission cross sections for excitation of the resonance transitions in Ba^+ ions by electron impact. The resonance transitions, between the excited $6^2P^o_{1/2}$ and $6^2P^o_{3/2}$ levels and the $6^2S_{1/2}$ ground state, produce photons with wavelengths of 4934 Å and 4554 Å. The thresholds for exciting the $6^2P^o_{1/2}$ and $6^2P^o_{3/2}$ levels are 2.5 eV and 2.7 eV, respectively. The

experimental results for the relative emission cross sections are presented in Tables 4 and 5 and in Figure 19. As shown in Figure 20, the relative data exhibit the high energy dependence predicted by the Bethe-Born approximation.[19] Over the energy range of the experiment, from 8 eV to 98 eV, the relative cross sections differ by approximately a factor of two, the ratio of the statistical weights of the 6P levels. The total error in the relative measurements varies from ±16 per cent to ±36 per cent. Of this error, ±6 per cent is systematic error in the measurement apparatus; there is also a systematic error, listed in Table 3, due to the possible dependence of the measured cross sections upon the residual pressure in the vacuum chamber. From a best estimate of the photon detection probability of the apparatus, estimated absolute emission cross sections are obtained; these data are presented in Tables 9 and 10. In addition to the total errors for the relative measurements, the estimated absolute cross sections contain a possible ±40 per cent error in the estimated photon detection probability plus a ±5 per cent error due to the polarization. Checks on the data were performed to evaluate the possible effects of such parameters as the beam intensities, beam modulation frequency, ion beam composition, ion beam energy, electron beam energy distribution, beam profiles, and signal-to-noise ratio.

The estimated absolute cross sections are compared with the theoretical predictions of Seaton[20] using the oscillator strengths and branching ratios of Gallagher[2] and estimating the cascading contribution to the resonance line emissions from the measurements of the excitation of cesium by electron impact of Zapesochnyi and Shimon.[35]

The agreement between experiment and theory for the magnitude and shape of the cross sections is remarkably good considering the 60 to 80 per cent error brackets on the experimental data and the 20 per cent error brackets on the theoretical curve due to the experimental determination of the branching ratios, oscillator strengths and cascading.

APPENDIX I

DERIVATION OF σ_{em} IN TERMS OF EXPERIMENTAL PARAMETERS

The number of photons per second per unit volume ϕ resulting from the collisions between ions and electrons can be obtained from the relationship

$$\phi = n_i \, n_e \, V_r \, \sigma_{em} \tag{A-1}$$

where n_i and n_e are the number densities of ions and electrons, respectively, V_r is the relative velocities of the intersecting particles, and σ_{em} is the cross section for the emission process. If ions and electrons move in mutually perpendicular, well collimated beams parallel to the X and Y axes, respectively, number densities and relative velocity can be computed from

$$n_i = \frac{J_i(y,z)}{e \, V_i} \tag{A-2}$$

$$n_e = \frac{J_e(x,z)}{e \, V_e} \tag{A-3}$$

and

$$V_r = (V_i^{\,2} + V_e^{\,2})^{1/2}, \tag{A-4}$$

Substituting these quantities into Equation (A-1) gives

$$\phi(x,y,z)\ dx\ dy\ dz = \frac{(V_i^2 + V_e^2)^{1/2}}{e^2\ V_i\ V_e}\ \sigma_{em}\ J_i(y,z)\ J_e(x,z)\ dx\ dy\ dz. \quad (A-5)$$

Integrating over the ion beam width along the Y axis and the electron beam width along the X axis gives

$$\phi(z)\ dz = \frac{(V_i^2 + V_e^2)^{1/2}}{e^2\ V_i\ V_e}\ \sigma_{em}\ i_i(z)\ i_e(z)\ dz \quad (A-6)$$

where

$$i_i(z) = \int_{y_i} J_i(y,z)\ dy \quad (A-7)$$

and

$$i_e(z) = \int_{x_e} J_e(x,z)\ dx. \quad (A-8)$$

The total currents of ions and electrons can be expressed in terms of $i_i(z)$ and $i_e(z)$ as

$$I_i = \int_{z_i} i_i(z)\ dz \quad (A-9)$$

and

$$I_e = \int_{z_e} i_e(z)\ dz \quad (A-10)$$

where z_i and z_e are the spatial extents of the ions and electrons, respectively, along the Z axis. It is convenient to express the total photon flux Φ_T in terms of the total currents. Such an expression is obtained by integrating Equation (A-6) and combining with Equations (A-9) and (A-10), i.e.,

$$\Phi_T = \frac{(V_i^2 + V_e^2)^{1/2}}{e^2 V_i V_e} \sigma_{em} I_i I_e F^{-1} \tag{A-11}$$

where

$$F^{-1} = \frac{\int_{z_{ie}} i_i(z)\, i_e(z)\, dz}{\int_{z_i} i_i(z)\, dz \int_{z_e} i_e(z)\, dz} \tag{A-12}$$

where z_{ie} is the region along the Z axis where nonvanishing current densities exist simultaneously.

Solving these equations for σ_{em} gives

$$\sigma_{em} = \Phi_T \frac{e^2 V_i V_e}{(V_i^2 + V_e^2)^{1/2}} \frac{F}{I_i I_e} \tag{A-13}$$

where

$$F = \frac{\int_{z_i} i_i(z)\, dz \int_{z_e} i_e(z)\, dz}{\int_{z_{ie}} i_i(z)\, i_e(z)\, dz} . \tag{A-14}$$

Let the range of integration in Equation (A-14) be uniformly partitioned into segments of lengths Δz. Then F may be approximated by

$$F \simeq \frac{\Delta z \sum_k i_{ik} \sum_k i_{ek}}{\sum_k i_{ik}\, i_{ek}} \tag{A-15}$$

where i_{ik} is the average ion current density in the k^{th} partition and i_{ek} is the average electron current density in the k^{th} partition.

If a movable slit scanner, with ion slit height h_i and electron slit height h_e, were positioned such that the slits were centered on the k^{th} partition, then

$$i_{ik} = \frac{\Delta I_{ik}}{h_i} \tag{A-16}$$

and

$$i_{ek} = \frac{\Delta I_{ek}}{h_e} \tag{A-17}$$

where ΔI_{ik} is the positive ion current passing through the ion slit in the k^{th} position and ΔI_{ek} is the electron current passing through the electron slit in the k^{th} position. Upon substitution of these expressions in Equation (A-15), the slit heights cancel and there results

$$F \simeq \frac{\Delta z \sum_k \Delta I_{ik} \sum_k \Delta I_{ek}}{\sum_k \Delta I_{ik}\, \Delta I_{ek}}. \tag{A-18}$$

Thus if the slit scanner is moved across the beams in uniform steps of length Δz, the resulting ion and electron currents, measured as a function of slit position, can be used in Equation (A-18) to calculate F. This last expression is the desired approximation to F. It is important to note that the only relevant dimension in this expression is the spacing between slit positions, Δz; other dimensions, such as the overall height of the ion beam and the heights of the scanning slits, cancel.

APPENDIX II

DEPENDENCE OF SIGNAL UPON MEASURED BEAM CURRENT DISTRIBUTIONS

From Equation (A-5) in Appendix I, the number of photons per second produced in the incremental volume at (x,y,z) is given by

$$\phi(x,y,z)\,dx\,dy\,dz = \frac{(V_i^2 + V_e^2)^{1/2}}{e^2\,V_i\,V_e}\,\sigma_{em}\,J_i(y,z)\,J_e(x,z)\,dx\,dy\,dz. \quad \text{(A-19)}$$

The signal or the number of counts per second, c(x,y,z), recorded from this photon flux is then given by

$$c(x,y,z)\,dx\,dy\,dz = P(x,y,z)\,\phi(x,y,z)\,dx\,dy\,dz \quad \text{(A-20)}$$

where P(x,y,z) is the probability that a photon emitted at (x,y,z) will be detected. The total count rate is thus given by

$$C_T = \frac{(V_i^2 + V_e^2)^{1/2}}{e^2\,V_i\,V_e}\,\sigma_{em} \int_{z_{ie}} \int_{y_i} \int_{x_e} P(x,y,z)\,J_i(y,z)\,J_e(x,z)\,dx\,dy\,dz \quad \text{(A-21)}$$

where x_e is the extent of the electron beam along the X axis, y_i is the extent of the ion beam along the Y axis, and z_{ie} is the region along the Z axis where nonvanishing current densities exist simultaneously.

Consider the integral

$$I = \int_{z_{ie}} \int_{y_i} \int_{x_e} P(x,y,z)\, J_i(y,z)\, J_e(x,z)\, dx\, dy\, dz. \qquad (A-22)$$

If the ion beam is uniform over its width along the Y axis and the electron beam is uniform over its width along the X axis, then

$$J_i(y,z) = c_y\, j_i(z) \qquad (A-23)$$

and

$$J_e(x,z) = c_x\, j_e(z) \qquad (A-24)$$

where c_y and c_x are the values of the currents along the Y axis and the X axis, respectively. From these equations the integral becomes

$$I = \int_{z_{ie}} c_y\, j_i(z)\, c_x\, j_e(z) \int_{y_i} \int_{x_e} P(x,y,z)\, dx\, dy\, dz. \qquad (A-25)$$

Performing the integration over x_e and y_i gives

$$\int_{y_i} \int_{x_e} P(x,y,z)\, dx\, dy = P_x\, x_e\, P_y\, y_i\, P(z) \qquad (A-26)$$

where P_x and P_y are the average values of $P(x,y,z)$ over x_e and y_i, respectively. Let

$$c_y\, y_i\, j_i(z) = i_i(z) \qquad (A-27)$$

$$c_x \, x_e \, j_e(z) = i_e(z) \tag{A-28}$$

and

$$P_x \, P_y \, P(z) = \eta(z) \tag{A-29}$$

where $\eta(z)$ is the average probability that a photon emitted in the z-plane of the collision volume will be detected. The integral I thus becomes

$$I = \int_{z_{ie}} \eta(z) \, i_i(z) \, i_e(z) \, dz \tag{A-30}$$

and the total count rate is given by

$$C_T = \frac{(V_i^2 + V_e^2)^{1/2}}{e^2 \, V_i \, V_e} \sigma_{em} \int_{z_{ie}} \eta(z) \, i_i(z) \, i_e(z) \, dz. \tag{A-31}$$

Assume that the electron beam is contained inside the ion beam, i.e., $z_{ie} = z_e$. Also assume the ion beam is uniform over the extent of the electron beam and has a value of i_i. In this case, the total count rate will be given by

$$C_T = \frac{(V_i^2 + V_e^2)^{1/2}}{e^2 \, V_i \, V_e} \sigma_{em} \, i_i \int_{z_e} \eta(z) \, i_e(z) \, dz. \tag{A-32}$$

Now consider the integral

$$I = \int_{z_e} \eta(z)\, i_e(z)\, dz. \tag{A-33}$$

If

$$\eta(z) = \frac{K}{z^2} \tag{A-34}$$

where K is a constant and z is now the distance from the plane of the limiting aperture of the detection system to the plane z in the collision volume, then

$$I = \int_{z_e} K\, z^{-2}\, i_e(z)\, dz. \tag{A-35}$$

If the maximum value of the electron linear current density occurs at $z = z_o$, then let

$$\eta(z_o) = K_o = K\, z_o^{-2} \tag{A-36}$$

and let

$$r = z - z_o \tag{A-37}$$

so that I becomes

$$I = \int_{-r_e}^{+r_e} \frac{K_o\, z_o^{\,2}}{(r + z_o)^2}\, i_e(r + z_o)\, dr \tag{A-38}$$

where r_e represents the largest extent of the electron beam away from z_o along the Z axis.

If $r_e << z_o$, then

$$K_o\left(1 + \frac{r}{z_o}\right)^{-2} \simeq K_o\left(1 - \frac{2r}{z_o}\right). \tag{A-39}$$

If $i_e(z)$ is symmetrical about z_o, or

$$i_e(r + z_o) = i_e(z_o - r) \tag{A-40}$$

then

$$I \simeq K_o \int_{-r_e}^{+r_e} i_e(r + z_o)\, dr \tag{A-41}$$

or

$$I \simeq K_o \int_{z_e} i_e(z)\, dz. \tag{A-42}$$

Thus if

(i) Both beams are uniform over their widths,

(ii) The electron beam is immersed in the ion beam,

(iii) The ion beam is uniform over the extent of the electron beam,

(iv) The electron beam is symmetrical about its maximum which occurs at $z = z_o$,

(v) The height of the electron beam along the Z axis is much less than z_o, the distance of the beam maximum from the limiting aperture of the photon detection system, and

(vi) The photon detection probability can be represented as

$$n = K_o z_o^2 z^{-2}, \qquad \text{(A-43)}$$

then only the average value of the photon detection probability over the collision volume at $z = z_o$ enters into the experimental determination of an absolute emission cross section.

The first approximation is discussed in detail in Chapter IV. That the next three approximations are valid is indicated by Figure 13 in Chapter IV and Table 12 in Appendix III. The electron beam maximum occurs at scanner position No. 14 in Figure 13 and at the corresponding position No. 940 in Table 12. This position is approximately 2.85 inches from the plane of the first lens of the detection system, which is the limiting aperture of the detection system. Since the height of the electron beam is less than 0.2 inches, approximation (v) is also valid. This approximation is improved by the fact that the electron current decreases rather sharply from its maximum value at $z = z_o$. Assumption (vi) was never proven although it should be a good first approximation.

If assumption (i) is not valid, then a three-dimensional form factor which determines the overlap of the beams and the photon detection probability will need to be measured as indicated by Equation (A-22). If assumption (i) is valid but the remaining assumptions are not, then the form factor will need to include the overlap of the beams

and the photon detection probability along the Z axis. This new form factor can be inferred from Equation (A-18) and Equation (A-33) as

$$F' = \frac{\Delta z \sum_k \Delta I_{ik} \sum_k \Delta I_{ek}}{\sum_k K_k \Delta I_{ik} \Delta I_{ek}} \qquad \text{(A-44)}$$

where K_k is the photon detection probability at the k^{th} position of the slit scanner. If the photon detection probability is uniform over the collision volume, then none of these modified form factors are necessary.

Assuming the photon detection probability varied as indicated by Equation (A-43) and normalizing K to 1.0 at scanner position No. 940, F' was computed for the data given in Table 12 in Appendix III and was found to differ from the indicated value of F by less than 0.5 per cent.

Shifting the electron beam current distribution by 0.040 inch, or two scanner positions, results in F' changing by about 3 per cent from the value calculated above. This indicates the importance of maintaining the same position of electron beam throughout the experiment.

APPENDIX III

TYPICAL EXPERIMENTAL PARAMETERS AND MEASUREMENT DATA

The experimental parameters used and the data taken during a typical run are presented in Tables 11, 12 and 13. The purpose of these data is to show typical operating conditions and data scatter during one run.

Table 11 gives typical filament currents and electrode potentials. The voltages to the extraction plate and to the analyzer plate are for an ion beam acceleration of 1000 volts.

The data from a typical scanning procedure are shown in Table 12. Note that the peak of the electron beam current distribution occurs at the 940 micrometer position. This position of the peak was maintained throughout the experiment so that the collision volume would remain at the same distance from the detection system.

A data run is shown in Table 13. Scaler 1 recorded the noise while Scaler 2 recorded the signal plus noise. The parameter SW indicates whether the electron beam is "on" during the first half of the ion beam cycle, SW = 1, or during the second half, SW = 2. The SIGNAL is the difference between Scaler 2 and Scaler 1, while S is the recorded counts per second derived by dividing the SIGNAL by the COUNTING PERIOD, T. The signal from the electron beam, σI_e, is recorded to facilitate checking the linearity of signal versus electron beam current. The cross section is calculated from the preceding data and the parameters

RUN NO. 104 - 1

ION SOURCE FILAMENT CURRENT	18	AMPS
ION SOURCE OVEN CURRENT	7.5	AMPS
ELECTRON SOURCE FILAMENT CURRENT	0.9	AMPS
VOLTAGE TO EXTRACTION PLATE	-50	VOLTS
VOLTAGE TO ANALYZER PLATE	+780	VOLTS
LOWER VERTICAL DEFLECTION VOLTAGE	0	VOLTS
UPPER VERTICAL DEFLECTION VOLTAGE	0	VOLTS
LEFT HORIZONTAL DEFLECTION VOLTAGE	+55	VOLTS
RIGHT HORIZONTAL DEFLECTION VOLTAGE	0-50 Pulse	VOLTS
VOLTAGE TO PM TUBE	+1800	VOLTS
AMPLIFIER GAIN	100	PER CENT
(INTEGRAL) (~~DIFFERENTIAL~~) MODE ON ANALYZER		
WINDOW HEIGHT ON ANALYZER	N/A	PER CENT

Table 11. Typical Voltages and Currents of Experimental Apparatus.

SCANNER DATA SHEET

REFERS TO DATA SHEETS 104 - 1

TAKEN (~~BEFORE~~) (AFTER) RUN NO. 241

	INITIAL	FINAL
I_i	4.4×10^{-8}	4.5×10^{-8}
I_e	0.30×10^{-3}	0.30×10^{-3}

MICROMETER POSITION	ΔI_e	ΔI_i	$\Delta I_e \quad \Delta I_i$
660	0.000×10^{-3}	0.00×10^{-9}	0.000×10^{-12}
680	.000	0.12	.000
700	.000	2.88	.000
720	.000	2.77	.000
740	.000	1.89	.000
760	.000	1.90	.000
780	.000	1.90	.000
800	.000	1.90	.000
820	.000	1.90	.000
840	.000	1.95	.000
860	.004	1.95	.008
880	.016	1.92	.031
900	.040	1.90	.076
920	.066	1.90	.125
940	.078	1.86	.145
960	.060	1.84	.110
980	.028	1.81	.051
1000	.007	1.80	.013
1020	.001	1.74	.002
1040	.000	1.69	.000
1060	.000	1.65	.000
1080	.000	1.61	.000
1100	.000	1.56	.000
1120	.000	0.79	.000
1140	.000	0.00	.000
0.020 INCH	0.300	41.23	0.561
ΔM	$\Sigma(\Delta I_e)$	$\Sigma(\Delta I_i)$	$\Sigma(\Delta I_e \quad \Delta I_i)$

$$F = \frac{2.54 \quad \Delta M \quad \Sigma(\Delta I_i) \quad \Sigma(\Delta I_e)}{\Sigma(\Delta I_e \quad \Delta I_i)} = \frac{2.54 \times 0.020 \times 0.300 \times 41.23}{0.561} = 1.120 \text{ cm}$$

Table 12. Typical Form Factor Data Sheet.

RUN NO. 104 - 1

DATE 4-26-67

ION VOLTAGE 1000; ION VELOCITY, V_i 3.75×10^{6}(cm/sec); ION PULSE PERIOD 20×10^{-3}(sec)

ELECTRON VOLTAGE 50; ELECTRON VELOCITY, V_e 4.19×10^{8}(cm/sec); ELECTRON PULSE PERIOD 10×10^{-3}(sec)

WAVELENGTH 4554 (Å); COUNTING PERIOD, T 900(sec); PRESSURE 8×10^{-9}(torr)

FORM FACTOR, F 1.120(cm); $\frac{e^2 V_i V_e}{(V_i^2 + V_e^2)^{\frac{1}{2}}} = 9.62 \times 10^{-32}$; $C = \left(\frac{e^2 V_i V_e}{(V_i^2 + V_e^2)^{\frac{1}{2}}} \times F \right) / I_i = 2.449 \times 10^{-24}$

ION CURRENT, I_i 4.4×10^{-8}(A); ELECTRON CURRENT, I_e 0.30×10^{-3}(A); APERTURE CURRENT 0.0085×10^{-3}(A)

RUN NO.	SW	SCALER 1	SCALER 2	SIGNAL	S	σI_e = CS	σ = CS/I_e	COMMENTS
241	1	71043	85719	14676	16.31	39.93×10^{-24}	13.31×10^{-20}	
242	2	68835	82106	13271	14.75	36.11	12.04	
243	1	67757	81827	14070	15.63	38.29	12.76	
244	2	67973	81234	13261	14.73	36.08	12.03	
245	1	36956	36990	+34	+0.04	+0.09	———	$I_e = 0$
246	2	67428	81705	14277	15.86	38.85	12.95	
247	1	67753	81703	13950	15.50	37.96	12.65	
248	2	67252	81739	14487	16.10	39.42	13.14	
249	1	67235	81898	14663	16.29	39.90	13.30	
250	2	64918	64378	-540	-0.60	———	———	$I_i = 0$

N_e = 31017 (N_e/I_e) = 3.4 $\langle \sigma I_e \rangle = 38.32 \times 10^{-24}$ $\langle \sigma \rangle = 12.77 \times 10^{-20}$

Table 13. Typical Cross Section Measurement Data.

listed above the data. The average value of σ is tabulated at the bottom of the data sheet; this is the average of the eight values of σ listed in the data. The experimental standard deviation for this run is ±4 per cent; whereas, the value of the standard deviation predicted by Equation (21) in Chapter III is ±3 per cent. Note also from Table 5 in Chapter IV that the standard deviation is ±5 per cent for all the data at 50 eV on the 4554 $\mathring{A}$ line. This indicates that most of the scatter in the data can be attributed to the Poisson statistics of the counting process.

The noise of the electron beam, N_e, is determined by subtracting the reading of Scaler 1 for Run No. 245 from the reading for Run No. 244. The electron noise parameter, (N_e/I_e), is derived by

$$(N_e/I_e) = \frac{N_e \times 3 \times 10^{-5}}{I_e \, T} \qquad \text{(A-45)}$$

$$= \frac{31017 \times 3 \times 10^{-5}}{0.30 \times 10^{-3} \times 900} = 3.4$$

Since this value is less than five, the data is valid according to the criterion discussed in Chapter IV.

BIBLIOGRAPHY*

1. C. Candler, Atomic Spectra, (D. Van Nostrand Company, Inc., Princeton, New Jersey, 1964), pp. 355.

2. A. Gallagher, Phys. Rev. 157, 24 (1967).

3. F. M. Bacon and J. W. Hooper, V International Conference on the Physics of Electronic and Atomic Collisions, Leningrad, U.S.S.R., July 17-23, 1967, Abstracts of Papers, (Publishing House "Nauka," Leningrad, 1967), pp. 41.

4. A. R. Lee and N. P. Carleton, Abstracts of Papers, 20th Annual Gaseous Electronics Conference; Bull. Amer. Phys. Soc. (To be published).

5. E. Hinnov, J. G. Hirschberg, F. W. Hofmann, and N. Rynn, Phys. Fluids 6, 1779 (1963).

   N. Rynn, E. Hinnov, and L. C. Johnson, Bull. Amer. Phys. Soc. 10, 213 (1965).

   N. Rynn, E. Hinnov, and L. C. Johnson, Rev. Sci. Instr. 38, 1378 (1967).

6. K. C. Rogers, "Drift Wave Instabilities and Plasma Diffusion Across a Magnetic Field," March 1965, Stevens Institute of Technology, Department of Physics.

7. K. T. Dolder, M. F. A. Harrison, and P. C. Thonemann, Proc. Roy. Soc. (London) A-264, 367 (1961).

8. M. F. A. Harrison, Brit. J. Appl. Phys. 17, 371 (1966).

9. W. C. Lineberger, J. W. Hooper, and E. W. McDaniel, Phys. Rev. 141, 151 (1966).

   J. W. Hooper, W. C. Lineberger, and F. M. Bacon, Phys. Rev. 141, 165 (1966).

10. G. H. Dunn and B. Van Zyl, Phys. Rev. 154, 40 (1967).

---

*Abbreviations used herein conform to those found in the American Institute of Physics Style Manual (1963).

11. D. F. Dance, M. F. A. Harrison, and A. C. H. Smith, Proc. Roy. Soc. (London) A-290, 74 (1966).

12. J. Tully, M. Sc. Dissertation, Univ. of London, (1960).

13. A. Burgess, Mem. Soc. Roy. Sci. Liege 4, 299 (1961).

14. S. Ormonde, W. Whitaker, and L. Lipsky, Phys. Rev. Letters 19, 1161 (1967).

15. D. P. Sural and N. C. Sil, Proc. Phys. Soc. (London) 87, 201 (1966).

16. O. Bely, Proc. Phys. Soc. (London) 88, 587 (1966).

17. P. G. Burke, J. H. Tait, and B. A. Lewis, Proc. Phys. Soc. (London) 87, 209 (1966).

18. H. Van Regemorter, Monthly Not. Roy. Astron. Soc. 121, 213 (1960).

19. H. Bethe, Ann. Physik 5, 325 (1930).

20. M. J. Seaton, Atomic and Molecular Processes, edited by D. R. Bates, (Academic Press Inc., New York, 1962), Chapter 11.

21. M. Gryzinski, Phys. Rev. 138, A305 (1965).

M. Gryzinski, Phys. Rev. 138, A322 (1965).

22. I. C. Percival and M. J. Seaton, Phil. Trans. A, 251, 15 (1958).

23. W. C. Lineberger, The Ionization of Lithium Ions by Electron Impact, (Ph.D. Thesis, Georgia Institute of Technology, Atlanta, Georgia, 1965).

24. R. H. Garstang and S. J. Hill, Pub. of Astron. Soc. Pacific 78, 70 (1966).

25. G. A. Harrower, Rev. Sci. Instr. 26, 850 (1955).

26. F. Rosebury, Handbook of Electron Tube and Vacuum Techniques, (Addison-Wesley Publishing Company, Inc., Reading, Massachusetts, 1965), pp. 98.

27. A. L. Hughes and V. Rojansky, Phys. Rev. 34, 284 (1929).

A. L. Hughes and J. H. McMillen, Phys. Rev. 34, 291 (1929).

28. P. Marmet and L. Kerwin, Can. J. Phys. 38, 787 (1960).

29. E. C. Yates, Rev. Sci. Instr. 36, 1883 (1965).

30. A. Papoulis, Probability, Random Variables and Stochastic Processes, (McGraw-Hill Book Company, New York, 1965).

31. R. M. Matheson, L. S. Nergaard, and R. H. Plumlee, R C A Review 18, 385 (1957).

32. J. S. Bendat and A. G. Piersol, Measurement and Analysis of Random Data, (John Wiley & Sons, Inc., New York, 1966), pp. 139.

33. H. Van Regemorter, Astrophys. J. 136, 906 (1962).

34. C. W. Allen, Astrophysical Quantities, second edition, (The Althone Press, University of London, London, 1963), pp. 42.

35. I. P. Zapesochnyi and L. L. Shimon, Doklady Akademii Nauk SSSR, 166, 320 (1966); English transl.: Soviet Physics-Doklady 11, 44 (1966).

VITA

Frank Mallary Bacon was born in Albany, Georgia on October 12, 1939. He is the son of R J and Carrie Harden Bacon.

Mr. Bacon attended public schools in Albany, Georgia and Sycamore, Georgia; he was graduated from Sycamore High School in 1957. He received the degrees of Bachelor of Electrical Engineering and Master of Science in Electrical Engineering in June, 1962 and June, 1964, both from the Georgia Institute of Technology.

Mr. Bacon was employed by the Electronics Division of the Engineering Experiment Station of the Georgia Institute of Technology from June, 1962 through December, 1963. Since January, 1964, he has held a Graduate Research Assistantship with the Engineering Experiment Station.

Mr. Bacon is a member of the American Physical Society, the Institute of Electrical and Electronics Engineers, and Sigma Xi.